TEMPORAL AND SPATIAL SCALES OF INFLUENCE ON NEARSHORE FISH SETTLEMENT IN THE SOUTHERN CALIFORNIA BIGHT

Jennifer E. Caselle, Brian P. Kinlan, and Robert R. Warner

Running title: Temporal and spatial scales of recruitment

Key words: recruitment, production, delivery, larval transport, dispersal, connectivity, fishes, spatial scale, temporal scale, kelp bass, rockfish, *Paralabrax, Sebastes*

ABSTRACT

Recruitment variation in marine populations is clearly affected by physical processes in the ocean. We therefore examined correlations between long-term, high-frequency data on fish settlement on artificial substrates and oceanographic processes operating at different spatial and temporal scales. We sought, for example, associations with processes occurring close in time and space to settlement events (suggesting processes affecting local delivery) or with those at particular spatial and temporal lags (suggesting influences on larval transport and survival or, at even greater time lags, on larval production). As examples, we used as response variables an 8-yr, biweekly record of settlement of three groups of fishes to sites in the Santa Barbara Channel, California, USA. Predictor variables were day-specific physical processes resolved to "local" scales and then binned and lagged to represent "regional" and "basin" spatial scales and more distant time horizons. We used linear models to assess the amount of variability in settlement associated with variation in processes at different spatial and temporal scales, representing different processes such as food availability or physical transport. We found that settlement is linearly associated with a combination of large-scale factors at long time lags, consistent with variation in production at sources and early larval survivorship, and with small-scale factors at short time lags, consistent with processes aiding delivery of competent individuals to suitable nearshore habitat. Species groups differ in the relative strength of these factors, potentially because of different biological attributes.

The proper scale of management has been a recent major focus of debate in fisheries science (Fogarty and Botsford, 2007). Traditional management, although recognizing variation among stocks, has usually taken the approach of managing all "stocks" or subpopulations of a species as a single unit (Hilborn and Walters, 1992). This approach rests on the assumption that fish populations are well mixed over large scales, at least at the time of settlement. Advocates of local management stress that population demography and processes such as settlement and recruitment may vary over small spatial scales and that management should reflect those scales (Prince, 2003; Gunderson et al., 2008). Of course, different population processes (such as larval dispersal and adult competitive interactions) probably occur at very different scales, so forcing factors operating at different scales (e.g., food availability for production of young and oceanographic features delivering those young) can act synergistically to control populations. The debate on the efficacy of local management will not be resolved until we know more about the relative contributions to population dynamics of forcing factors occurring at a wide range of spatial and temporal scales. Here we demonstrate a technique for identifying the relative contributions of a variety of forces to one important population process, settlement to the nearshore environment.

Settlement of marine organisms is clearly affected by physical processes in the ocean, but the exact roles of these processes, and the scales over which they act, remain obscure (Warner and Cowen, 2002; Sale et al., 2005; Siegel et al., 2008). Successful settlement of reef-based organisms is influenced by a wide variety of forces, beginning with production and ending with delivery of individuals to a reef (Sponaugle et al., 2002). In between, while in the plankton, larvae also disperse, grow, and die. Recruitment to the population or fishery occurs at some point after settlement and is likely to be influenced by postsettlement processes, such as density-

dependent mortality, movement, and/or growth (Carr and Syms, 2006), that we did not measure. Variation in rates of settlement and recruitment has been well established to drive population dynamics of benthic marine organisms (Roughgarden et al., 1988). The literature on recruitment variability in marine organisms is enormous, and although many studies have made important progress on explaining patterns in time and space, the focus is often limited to one or a few discrete spatial and temporal scales. For coral-reef fishes, many good examples of fine-scale temporal recruitment patterns appear in the literature (Victor, 1986; Doherty et al., 2004; Anderson et al., 2007), but these studies are often limited in spatial scale. For temperate reef fishes, the causes are generally even less well known, and studies tend to be even more limited in time and space (Carr and Syms, 2006), often dealing with annual variation in year-class strength. Although important for fisheries management, measurements of year-class strength alone preclude detailed understanding of the influence of physical oceanographic effects on transport and settlement of early life-history stages by confounding these effects with postsettlement, reef-based mortality.

Combination of high-resolution settlement data with fine-scale indices of potential physical and biological mechanisms may help elucidate the processes that control settlement at a variety of spatial and temporal scales. Here, we present long-term, high-frequency fish settlement data and develop indices of bio-physical processes occurring at a range of spatial and temporal scales and lag times/distances from the point of settlement. We then apply a simple regression-based approach to describe the linear association of settlement with potential predictors. We find strong association between bio-physical processes and daily settlement rates at a wide range of time and space scales and lags. The picture that emerges is one of a complex, multi-scale interplay of spatial and dynamic processes operating at different phases of pre-

settlement life history, and differing among species in relation to their life history traits. In particular, our results illustrate the importance of including information at multiple time and space scales and lags, and of including indices of wind-driven circulation processes in this temperate coastal upwelling system. Given the complexity of the underlying dynamic processes, we avoid using the simple linear regression techniques developed here for prediction or mechanistic inference. Instead, we conclude with a brief discussion of other analytical techniques better suited to building a predictive, mechanistic understanding of recruitment dynamics.

METHODS

Response variables in our study were 8-yr records of settlement of the three groups of fish species most frequently collected. Predictor variables were day-specific physical and biological processes (wind-driven circulation metrics, temperature, and chlorophyll) resolved to "local" scales (10-12 km) and then binned and lagged to represent events occurring at larger "regional" (~250-km) and "basin" (~500–750-km) spatial scales and more distant time horizons. For each species group, we asked how much of the variability in settlement (both spatial and temporal) is associated in a simple linear way with physical or biological processes occurring at different spatial and temporal scales and representing different processes, such as food availability or final delivery of settlers to a site (Fig. 1).

Settlement Monitoring

We monitored arrival of newly settled reef fishes on artificial collectors known as SMURFs (standard monitoring units for recruitment of fishes; Steele et al., 2002; Ammann, 2004) at 14 sites throughout the Santa Barbara Channel (SBC) and northern Channel Islands (Table S1, Fig. 2A, Fig. S1), southern California, USA. Because settlement to SMURFs is

independent of the availability or quality of nearby settlement habitat, SMURFs estimate the relative abundance of competent individuals (pelagic juveniles in the case of one rockfish group) available for settlement at a site, not necessarily the number of individuals that actually choose to settle to natural substrates (Steele et al., 2002; Ammann, 2004; J. E. Caselle, unpubl. data). Here, we use the term "settlement" to mean the rate at which young fish appeared on the SMURFs.

The artificial collectors also provide a better estimate of settlement than visual surveys of postsettlement fish on the reef because they minimize the effects of variation in natural habitat and consistently collect the smallest, youngest settlers without substantial postsettlement mortality (Ammann, 2004; White and Caselle, 2008). At each site, three replicate SMURFs were placed on separate mooring lines 500 m from one another and 200–500 m offshore of kelp beds at sites where kelp was present or, elsewhere, 200–500 m from shore. All moorings were located in approximately 15 m of water, and SMURFs were placed 3 m below the surface buoy. We collected fish settlers from each SMURF biweekly (approximately first quarter and third quarter moons) from April through November from 2000 to 2007 (Table S2 gives the dates over which each site was sampled and number of samples per year; see White and Caselle, 2008, for methods). Earlier studies with daily sampling regimes indicated that biweekly sampling is sufficiently frequent to minimize postsettlement mortality on SMURFs (Steele et al., 2002; Ammann, 2004).

Circulation in this region is dominated by the cold California Current, flowing equatorward past Point Conception and the western Channel Islands, and the warm Davidson Current, flowing poleward along the coast and bathing the easternmost Channel Islands. During the summer and fall, the channel experiences persistent, cyclonic, eddy-like circulation and a sea-surface temperature front (Harms and Winant, 1998).

Species and Species Groupings

The most abundant settlers to SMURFs in Southern California are two groups of rockfishes (genus *Sebastes*) and a warm-temperate serranid, the kelp bass (*Paralabrax clathratus* (Girard, 1854)). These groups differ importantly in planktonic larval duration (PLD), size at settlement, and timing of both spawning and settlement, so they are ideal for comparing the effects of physical processes on settlement. Despite differences in life-history characteristics, these species occupy similar adult and juvenile habitat, consisting of nearshore rocky reefs and kelp forests (Miller and Lea, 1972; Love et al., 2002).

The kelp bass, found predominantly from Point Conception to Punta Abreojos along the west coast of North America (Young, 1963; Miller and Lea, 1972; Love, 1996), is a common inhabitant of mainland and island rocky reefs in southern California, especially in the eastern part of the study area. Although the species spawns from the late spring to early fall, reproduction in southern California peaks in June–August (Erisman and Allen, 2006). Kelp bass are broadcast spawners. Fish aggregate and externally broadcast eggs and sperm into the water column, where fertilization takes place. Individual females may spawn every 2–5 d during the spawning season (Oda et al., 1993; Erisman and Allen, 2008). The larvae settle to shallow rocky reef and kelp-forest habitat in the late summer and early fall (Findlay and Allen, 2002) at approximately 8–10 mm standard length after spending three to four weeks in the plankton (mean PLD = 27.9 d; Findlay and Allen, 2002; Shima and Findlay, 2002).

Rockfishes are a speciose group of cold-temperate fishes, most common in the northeast Pacific (Love et al., 2002). Unlike kelp bass, rockfishes are internally fertilized and release feeding larvae; gestation period probably depends on temperature (Sogard et al., 2008). Females of the species we studied are thought to release larvae once per season (Romero, 1988; Larson,

1992; Gilbert et al., 2006). Newly settled rockfish are also more fully developed (i.e., in pigmentation, fin development, eye development) than kelp bass and are probably stronger swimmers (pers. obs.). Two groupings of nearshore rockfishes settled to SMURFs in the study region, each with a distinct set of shared morphological and life-history characteristics.

The KGB group includes kelp, gopher, and black-and-yellow rockfishes (*Sebastes atrovirens* (Jordan and Gilbert, 1880); *S. carnatus* (Jordan and Gilbert, 1880); and *S. chrysomelas* (Jordan and Gilbert, 1881)). These species range from northern California to central Baja California. KGB rockfishes release larvae from late winter through spring, and fish settle to kelp canopy and rocky reef habitat after larval durations of approximately 1–3 mo (Moser, 1996; Gilbert, 2000) at lengths of less than 2 cm total length. Settlement occurs from midsummer through the fall (Anderson, 1983, Love et al., 1990; Carr, 1991).

The OYT group consists of two species, the olive and yellowtail rockfishes (*Sebastes serranoides* (Eigenmann and Eigenmann, 1890) and *S. flavidus* (Ayres, 1862)). We suspect that the majority of settlers in our study were olive rockfish, given the distribution and abundance of adults (Love et al., 2002), but the two species share similar larval characteristics including larval release during the winter, pelagic duration of 3.5–4 mo, and large size at settlement (2.8–5 cm total length). In addition to a planktonic larva, OYTs have a pelagic juvenile stage that the KGBs do not share (Moser, 1996). Although this group is reported to settle from spring through the fall (Love et al., 2002), we observed OYTs to settle only in the spring in our study area.

Analysis

Predictor Datasets.—We used satellite-based measurements of surface winds, temperature, and chlorophyll concentration to develop indices of circulation, thermal environment, and phytoplankton abundance, respectively, for each of our regions of interest (Figs. 2B, 3) and at the

set of sample-site point locations (Figs. 2A, 4, S1). Transport by surface currents, temperature, and food availability are all hypothesized to affect one or more phases of production and development (Fig. 1). The result was a set of "potential predictor variables" detailed in the Appendix. All predictor variables were derived from available global oceanographic databases as follows.

Wind-driven circulation: We derived indices of wind-driven circulation and transport by combining blended satellite/model wind data for our region (~50-km resolution), digital coastlines (1-km resolution), and the fundamental equations describing wind-driven coastal upwelling in deep water of constant density. These indices should be considered idealized proxies for actual upwelling and downwelling, which are influenced by a host of other factors either not included in the simple equations we used to describe transport (e.g., shallow-water bathymetry, stratification) or not resolved by the relatively coarse wind data (e.g., effects of mesoscale and submesoscale eddies and topographic features on actual wind stress and curl). These indices could be greatly improved by more realistic circulation models, finer-scale wind data, and validation against observations of surface and subsurface circulation in our study region. In general, the temporal pattern of the indices is probably more reliable than the absolute magnitude of transport estimates, because of bathymetric, sub-grid-scale, and other effects acting to damp or enhance the effects of regional-scale wind stress. Nonetheless, we applied them here to demonstrate that even relatively simple spatiotemporal indices of circulation processes can improve our ability to resolve processes important to settlement. Importantly, the method we describe here can be applied to any coastline in the world below ~60° latitude (above this level, the quality of scatterometer wind data is lower) through use of only the existing, publicly available data referenced below.

The QuikSCAT/NCEP blended wind product, available at http://dss.ucar.edu/datasets/ds744.4/, combines all available rain-corrected and quality-controlled QuikSCAT satellite scatterometer observations of sea-surface winds (~25-km native resolution) with National Center for Environmental Prediction (NCEP) Climate Data Assimilation System global gridded wind fields (~1.9° or 200-km resolution) to produce a gap-free, global, 6-hourly, 0.5° × 0.5° (~55-km in the vicinity of our study) gridded dataset of *u* (east-west) and *v* (north-south) components of sea surface (10-m height) wind-velocity vectors (Fig. 5A) and wind-stress curl (Fig. 5C) (Milliff and Morzel, 2001). Coverage is from August 1999 to March 2008. Daily averages of 6-hourly wind fields were calculated and smoothed in the time domain with a 5-d backward-looking rectangular moving-average filter to focus on time scales over which substantial adjustment of surface flow to upwelling-favorable winds is expected. Wind stress ($\boldsymbol{\tau}$) was calculated from wind velocity vectors (with the empirical wind-stress equation of Large et al., 1994) and used to calculate theoretical volume transport due to Ekman transport as follows:

$$\text{Ekman transport} = \boldsymbol{\tau}_{along}/(\rho \cdot f_0) \quad (\text{m}^3 \cdot \text{s}^{-1} \cdot \text{m coast}^{-1}) \qquad (1)$$

where ρ is the density of seawater, f_0 is the local value of the Coriolis parameter, $\boldsymbol{\tau}_{along}$ is the component of the wind stress vector parallel to the local coastline orientation, and Curl($\boldsymbol{\tau}$) is the curl of the wind-stress vector, calculated by a numerical method described by Milliff and Morzel (2001) and distributed as part of the QuikSCAT/NCEP blended wind product. Similarly, the curl of the wind stress (distributed as part of the QuikSCAT/NCEP product and also based on the wind-stress equation of Large et al., 1994) was used to calculate theoretical volume transport due to Ekman pumping:

$$\text{Ekman pumping} = L\ \text{Curl}(\boldsymbol{\tau})/(\rho \cdot f_0) \quad (\text{m}^3 \cdot \text{s}^{-1} \cdot \text{m transect}^{-1}) \qquad (2)$$

where L is the length of a hypothetical cross-shore (shore-normal) transect over which the

vertical velocity due to Ekman pumping is integrated to yield a volume transport due to Ekman pumping in the same units used for Ekman transport. For the work reported here, we assumed L = 100 km so that values of our Ekman-pumping index would be (arbitrarily) of the same magnitude as the Ekman transport index. Coast orientation was determined from a 1:250,000 world vector shoreline discretized at 1-km intervals (Soluri and Woodson, 1990). The orientation of 1-km segments was averaged over a 100-km window centered on the point of interest for the mainland coastline (10 km along island coastlines). Calculated transports were not highly sensitive to changes in the size of the window used to determine coast orientation (Table S1).

Some difficulty arises when the spatial scale of the resulting transport estimates is considered, because 1-km coastline data are combined with gridded wind data with a nominal resolution of ~55 km (itself derived from a blend of ~25-km satellite observations and scattered point observations of wind assimilated into the ~200-km grid of the NCEP climate model). Spatial autocorrelation analysis of the transport estimates (not shown) suggested that indices contained at least some nonredundant information down to scales of ~5–15 km. Hereafter we refer to the nominal scale of the wind-driven circulation indices as ~10 km, but the reader is reminded that these indices probably neglect important information at scales below the 55-km resolution of the wind product.

The long term (1999 to 2008) mean daily wind velocity field, transport estimate, curl of the wind stress, and pumping estimate are shown in Figs. 5A, B, C, and D, respectively. Daily transport, pumping, and offshore wind estimates were calculated at each site location (Fig. 4, S1). We also calculated mean daily Ekman transport and Ekman pumping estimates for each of the three regions by averaging daily values at all 1-km-spaced coastal grid locations within the region (Fig. 3G–L).

Larval settlement may be affected in qualitatively different ways by upwelling and downwelling processes, as well as by the spatial distribution of upwelling and downwelling within a region. We therefore employed a set of indices that separately measured total upwelling and total downwelling expected to occur (given our idealized assumptions) in a given region on a given date. For example, we produced daily estimates of total "spatially integrated" upwelling due to Ekman transport by integrating (summing) volume transports at points at 1-km intervals along all coastlines in each of our regions of interest, ignoring values less than 0. We followed a similar procedure for Ekman pumping and repeated the calculations for downwelling (using only values of transport or pumping less than or equal to 0).

Sea Surface Temperature (SST): We assessed the thermal environment at site locations (local SST) and in each of our three regions of interest (regional and basin-scale SST) using 5-d composite sea surface temperatures from Pathfinder 5 AVHRR 4-km gridded satellite images (available at http://www.nodc.noaa.gov/sog/pathfinder4km). We used the average of night and day 5-d composites and linearly interpolated to a daily interval for comparison with other sets of data (recognizing that we will be unable to resolve time-lag differences smaller than 5 d in correlation analyses involving SST variables). For site locations, we used the mean SST in a 3- × 3-pixel (= 12- × 12-km) rectangle centered as closely on the site as grid resolution allowed. The 3- × 3-pixel average was found to be more stable and to provide a more continuous time series than resulted if only the single pixel closest to the site was used. The resulting site time series are shown in Fig. 4 and in Fig. S2. Regional temperatures were calculated in the same manner but averaged over the entire region of interest (Fig. 3A–C).

Surface Chlorophyll-*a* Concentration: We described pelagic primary productivity in our three regions of interest using surface chlorophyll *a* (Chl) concentration from SeaWiFS (sea-

viewing Wide Field-of-View Sensor, GeoEye, Dulles, Virginia, USA). We used the 8-d, 4-km standard mapped images available for research use (http://oceancolor.gsfc.nasa.gov/SeaWiFS/). Values of the Chl-concentration-derived parameter were averaged over the region and interpolated to daily time interval (note was taken of limitations on time-lag resolution similar to those for SST data). The resulting resampled daily time series of average Chl for each region is shown in Fig. 3D–F.

Identification of Predictor Variables.—Lagged cross-correlations of daily time series of settlement for each of the three species groups and predictor variables were calculated for each response variable at each site for lags from 0 to 150 d (see example, Fig. 6), a range chosen on the basis of the life histories of our taxa of interest. Response variables for all analyses were $\log_{10}(x + 1)$-transformed daily settlement-rate time series. Although an inherent 14-d smoothing is introduced by the interval between SMURF collections, data were treated as point estimates of the settlement rate on the day of collection for purposes of regression and correlation, so that individual data would not be reused.

We first visually examined the daily lagged correlation plots for each predictor and response variable to choose the length of a "time integration window" (rectangular moving average filter applied to the predictor data series) that maximized the magnitude of significant peaks and/or troughs in the autocorrelation function across most or all sites. We tested the sensitivity of our choice of window size by using windows 25–50% above and below the specified size and found that the results were not sensitive to the window size within this range.

Next, new lagged correlation plots were calculated from predictor time series smoothed with a rectangular moving average filter of the chosen length. If fewer than two sites had significant correlations at any lags, the predictor was excluded. Otherwise, peak lags were

identified according to the following algorithm:

1. Identify contiguous intervals of the time-lag axis over which at least one site exhibited significant correlation with the predictor at the $P < 0.05$ level (uncorrected for multiple testing) and all adjacent significant correlations were of the same sign. If multiple intervals existed for a given species-predictor combination, then steps 2 and 3 (below) were repeated for the two intervals with the largest average peak correlation (as calculated in step 3), resulting in two predictors corresponding to two different time lags. We discarded other intervals of correlation to avoid problems with nonindependence that could result from inclusion of many predictors derived from the same underlying series of data.

2. Find the subset of time lags in the interval from (1) with the highest frequency of significant correlations among all sites.

3. From the time lags in the subset identified in (2), choose the one at which the arithmetic mean of the magnitudes of all correlations (i.e., averaged over all sites) is largest.

Finally, we screened the predictor set to reduce the most obvious multicollinearities. This screening was done without inclusion of interactions (i.e., by a stepwise regression approach), with the goal of identifying and removing the largest first-order collinearities. Such collinearities mainly occurred with SST, which had a strong, smooth, regular seasonal cycle. Dropping SST-related predictors, and in some cases selected transport or chlorophyll predictors, reduced collinearity and improved the stepwise regression model, as gauged by lower values of the Akaike information criterion (AIC).

Regression Model.—Applying the above criteria to identify predictors led to a different set of final predictor variables for each species group (Tables 1, 2, 3). For each species, all identified predictor variables and all possible centered two-way interactions were included as continuous

predictors in a multiple linear regression with a fixed effect (site). The site effect represents unaccounted-for time-invariant differences among sites. Inclusion of two-way interactions reduced the likely impact of collinearity on the whole-model fit, but caution should be used in interpreting main effects and interaction effects (if two variables are partly collinear, one may enter as a main effect and the other in a significant interaction, when the opposite could have occurred if the variance structure of the two time series were slightly different). Rather than focusing on interpretation of individual significant effects or using this model for prediction, we simply use it as a descriptive tool to summarize the percentage of variance explained by groups of effects on the basis of their associated time scales and process categories (Tables 1, 2, 3 and the Appendix). The fraction of model variance attributed to different spatial scales, time scales, and processes was estimated by addition of the sums of squares for model effects at a given space or time scale or associated with a given process and division by the model (not total) sum of squares. The spatial scale of interaction effects was defined to be the smaller of the two interacting scales. We estimated the nominal time scale associated with each predictor using the following formula (Effect 2 is ignored for noninteraction terms):

$$\left| \min\left\{\text{med}\left\{PSlag_{\max}^{Effect1}, PSlag_{\min}^{Effect1}\right\}, \text{med}\left\{PSlag_{\max}^{Effect2}, PSlag_{\min}^{Effect2}\right\}\right\}\right| + \max\left\{T_{\text{int}}{}^{Effect1}, T_{\text{int}}{}^{Effect2}\right\}$$

Here min, max, and med represent the minimum, maximum, and median, respectively, and *PSlag* variables denote the range of possible true presettlement time lags. We estimate presettlement lags from the time integration window (T_{int}) and time *lag* (Tables 1, 2, 3), taking into account the smoothing introduced by the 14-d collection interval:

$$PSlag_{\max} = lag - T_{\text{int}} + 1$$

$$PSlag_{\min} = \min\{0, lag - T_{\text{int}} + 15\}$$

For example, if the lag used in analysis was *lag* = –18 d for a predictor variable *X* smoothed with

a T_{int} = 5-d moving average, [$PSlag_{min}$, $PSlag_{max}$] would be [–22, –8]. A positive correlation between predictor *X* and settlement would indicate a positive relationship between changes in *X* and settlement events that occurred anywhere from 8 to 22 d later. The nominal time scale associated with *X* would be 20 d. Given the smoothing of predictor data and uncertainty in lag time between settlement and SMURF collection, nominal time scales are approximate and used only for purposes of binning effects in broad intervals (5–30 d) for examination of the qualitative pattern of variance explained at different time scales.

To assess the justifiability of including predictors from all spatial scales, we created a set of reduced models by progressively eliminating explanatory variables from the full model, starting with variables associated with the largest spatial scale (region), and finally eliminating the smallest (local) variables, leaving only the fixed site effect. This process served two purposes. First, it allowed us to compare AICs for the full model used in the rest of our analyses to reduced models. The full model for each species had a lower AIC than any of the reduced models created in the manner described above, supporting the hypothesis that the additional variance explained by the full model justified its complexity. Second, it provided another measure of the variance explained by processes operating at different spatial scales: the average pairwise difference in R^2 values between models that included a given spatial scale and reduced models without predictors at that spatial scale.

The assumptions underlying conventional parametric significance tests are violated by the auto- and cross-correlated nature of predictors and autocorrelation of responses, unbalanced temporal and spatial sampling, and preselection of particular lags and smoothing scales for predictors intended to maximize correlation with the response. We addressed these issues by replacing standard distribution-based significance tests with Monte Carlo P-values derived from

simulated distributions of each test statistic under the null hypothesis of no association between environment and settlement. For this analysis, predictor data series were unchanged, so they retained all idiosyncrasies of the data, including auto- and cross-correlation, effects of temporal and spatial gridding and smoothing, and effects of time-integration windows and lag selection. We then inferred autocorrelation functions from the original settlement time series by semivariogram analysis (Deutsch and Journel, 1998; see Fig. S3) and used unconstrained sequential Gaussian simulation (Deutsch and Journel, 1998) to produce 1000 random "null" response data sets that reflect the autocorrelation functions of the actual data but are otherwise unassociated. The regression model was fit to each null data set, and the empirical distribution of the statistic of interest formed the basis for Monte Carlo significance tests including P-values and 95% confidence intervals of parameters under the null hypothesis. All P-values reported in regression tables were derived by this technique, rather than from the standard parametric statistical tests. This practice protects against spurious significant results that might arise from constraints imposed by the multiple types of nonindependence exhibited by our data and also corrects for deviations from multivariate normality and heteroscedasticity. The whole-regression-model P-values were constructed by comparison of actual to simulated F-ratios and R^2 values (which gave the same qualitative results). P-values for variance fractions were constructed by comparison of the actual percentage of the total variance represented by the sums of squares for each process, space, or time-scale grouping to the simulated values.

In addition to rejecting the null hypothesis of no association, we were concerned with the uncertainty of model estimates when a significant association exists. Parametric estimates of standard errors also depend on normality and independence assumptions violated by our data. We therefore employed a bootstrap method to characterize uncertainty in variance fractions,

parameter estimates, and other model outputs. We constructed 1000 random subsets, each containing 90% of the data points, fit the model to each subset, and used the 2.5 and 97.5 quantiles of the resulting empirical distribution of each model output to define bootstrap 95% confidence intervals.

Finally, the bootstrap model fits permit cross-validation by using models fitted to each randomly selected subsample of data ("training set") to predict data that were excluded ("validation set"). Although our focus is not on prediction, cross-validation R^2 statistics are useful for assessment of the robustness of the model as a general description of patterns of association between predictors and responses that are robust to outliers and idiosyncratic subsets of the data. Using the 1000 models fit to random subsets (90% of data) for bootstrap analysis, we predicted each corresponding validation data set (10% of data not included in the model fit) to calculate the empirical distribution of the cross-validation R^2 statistic. We summarize this distribution by the mean and 95% confidence interval (2.5 and 97.5 quantiles).

RESULTS

Variable selection

The variable-selection procedure resulted in a number of continuous predictors that entered the full regression model (kelp bass = 18, KGB group = 13, OYT group = 17). All models also included a fixed site effect with 14 levels (the 14 sampling sites), and all possible two-way interactions of continuous predictors. Exact time integration windows and lags used for significant predictors are reported in Tables 1, 2, and 3. To reflect uncertainty in true time lags relative to settlement, we refer below to approximate presettlement time lags calculated as described in Methods.

Kelp Bass.—For kelp bass, 18 continuous predictor variables were included in the full

regression model. SST entered the models at the site scale (lag <2 weeks) and at central and south regional scales (lags of 3–4 weeks), as did offshore wind stress and Ekman pumping at the site scale (lags <2 weeks). We included regional Chl from all regions with lags of <2 weeks as well as lags of ~4–5 mo for the central region and ~3 mo for the north. Downwelling pumping in all three regions, again with shorter lags in the central and south (<2 weeks) and a longer lag in the north (~4 mo), was also included. Downwelling transport was correlated with settlement only in the central region at a lag of <2 weeks, whereas upwelling transport was correlated at lags <2 weeks for north and central regions, and 2–4 weeks for the south. Ekman transport in the central and north region was included with lags <2.5 weeks.

KGB Group.—For the KGB rockfish group, 13 predictor variables were included in the full regression model. SST entered the model for the central region only with a lag of 1–2 mo. Ekman pumping, SST, and offshore wind stress at the site scale entered the model with lags <2.5 weeks. Chlorophyll in the central region was correlated with settlement at lags of ~2 mo and ~4–5 mo, and in the south region at a lag of ~1 mo. Downwelling pumping in all three regions was correlated with settlement, at generally longer lags than for the kelp bass (central ~2 mo, north ~1 mo, and south ~4 mo). Downwelling transport and upwelling pumping in the central region entered the model with lags of ~4 mo and <2 weeks, respectively. Ekman transport also entered the model for the central region only with a lag of ~2 mo.

OYT Group.—For the OYT rockfish group, 17 variables were included in the full regression model. OYT settlement was correlated with SST in the central region with a lag of 1–3 weeks. Regional Chl from all three regions was included, with two distinctly longer lags in the central region (~1 and ~4 mo) and shorter lags in the south and north regions (<2.5 weeks). Ekman pumping, Ekman transport, and offshore wind stress at the site scale entered the model with lags

of <2 weeks. Site-scale SST entered at a lag of 3–4 weeks. Downwelling pumping in all three regions was correlated with settlement; lags were shorter in the north (2–4 weeks) and longer in the central and south (1.5–2 and 3–3.5 mo). Ekman transport showed a similar pattern at the regional scale; lags were shorter in the north (<2 weeks) and longer in the central and south (~2 mo and ~1 mo). Downwelling transport and upwelling transport in the central region were both correlated with settlement of the OYT group with lags of ~3.5 and ~2 mo, respectively.

Regression model results

Kelp Bass.—The kelp-bass regression model was significant (Monte Carlo $P < 0.0001$) and explained 57% of the variance in settlement (Table 1). Of the 18 predictor variables selected to enter the regression model, 12 were involved in effects (main or interaction) that were significant at the $P < 0.05$ level, four of which were robust in cross-validation (Table 1). The fixed site effect was also significant and robust. Of the significant main effects in the model, three were related to regional- and basin-scale wind and circulation, one to basin-scale food, and one to basin-scale temperature. When cross-validation parameter estimates were considered, the most robust effects were downwelling transport in the central region and Chl in the south.

Ten two-way interactions were significant ($P < 0.05$), involving primarily wind and circulation processes and food at basin to regional scales but also involving temperature and offshore wind stress at the site scale. The most robust two-way effects were interactions between site-scale SST and downwelling pumping in the north region and Chl in the central and south regions.

KGB Group.—The KGB regression model was significant (Monte Carlo $P < 0.0001$) and explained 60% of the variance in settlement (Table 2). Of the 13 predictor variables selected to enter the regression model, 11 were involved in effects (main or interaction) that were significant

at the $P < 0.05$ level, three of which were robust in cross-validation (Table 2). The fixed site effect was also significant and robust. Only one predictor, offshore wind stress at the site scale, was significant as a main effect; it was also robust. Wind and circulation variables were involved in every significant effect (main or interaction), primarily at the site or regional scale. Overall, 11 interaction effects were significant ($P < 0.05$). Only two of these were robust, and these were restricted to the central region: downwelling pumping × upwelling pumping and Chl × downwelling transport.

OYT Group.—The OYT regression model was significant (Monte Carlo $P < 0.0001$) and explained 60% of the variance in settlement (Table 3). Of the 17 predictor variables selected to enter the regression model, 13 were involved in effects (main or interaction) that were significant at the $P < 0.05$ level, two of which were robust in cross-validation (Table 3). The fixed site effect was not significant. As for kelp bass, significant predictors (main effects and interaction terms) occurred in all "process" categories: wind/circulation, temperature, and food. Of the five significant main effects, two were related to food at the regional scale and two to temperature at site and regional scales. The only robust main effect was Chl in the central region.

As was the case for KGB rockfish, wind and circulation processes were involved in every significant interaction term, but the basin scale occurred more commonly than for the KGB group. The only robust interaction was between Ekman pumping at the site scale and downwelling pumping in the north region.

Variance Fractions Binned by Space, Time, and Process

Each of the three fish groups showed clear differences in the proportion of variance associated with proxies for different processes acting at different spatial scales and times before settlement. For ease of interpretation, we have summarized the variance explained by significant

effects from the models by "binning" (summing) over space (Fig. 7A–C) and time (Fig. 7D–F) scales, as well as by process categories (Fig. 7G–I). Because the proportion of unexplained variance was similar for all species groups, bars in Fig. 7 show the percentage of *model* variance (not total variance) attributed to each category.

Time Scales.—Variance in KGB rockfish settlement was explained primarily by factors acting immediately (<2 weeks) before settlement and long (~2–5 mo) before settlement, corresponding to periods during and before production of larvae by females (Fig. 7D). In contrast, settlement in the OYT rockfish group was influenced by factors acting at intermediate time scales, ~1–3 mo before settlement, the period corresponding to parturition and larval life (Fig. 7E). Factors acting just before settlement had very little effect on this group. The kelp bass was mainly affected by processes immediately (<2 weeks) before settlement and at lags corresponding to pelagic larval life for this species (2 weeks to 2 mo; Fig. 7F). Factors occurring much before settlement (lags >2 months) were less important to settlement of this species.

Space Scales.—Because of the coarseness of spatial scales in our analysis, we estimated the spatial variance fractions by two different methods—sums of squares and hierarchical model comparison (see Methods) and averaged the results. Confidence intervals were chosen to be the larger of the cross-validation 95% CI for the sum of squares method and the standard deviation of the values given by the two methods (Fig. 7A–C).

By either method, the fixed site effect accounted for less variance than local and regional effects for all species, lowest for OYT and similar for KGB and kelp bass (Fig. 7A–C; mean of two methods = 17% for KGB, 4% for OYT, and 19% for kelp bass). Factors acting at the regional scale (i.e., in the central region, containing the study sites), explained the most variance relative to local and basin scale factors for all three groups (Fig. 7A–C; means = 53% for KGB

and OYT and 39% for kelp bass), but basin-scale factors were relatively more important for kelp bass (mean = 21%) and OYT rockfish (17%) than for KGB rockfish (6%). Local-scale factors were associated with a similar fraction of model variance for all groups (means ranged from 20 to 25%).

Process Categories.—We calculated the percentage of model variance associated with each process category by the same procedure as for temporal scales (Fig. 7G–I). The striking result is that wind and circulation processes, either alone or in an interaction term with food or temperature, explained the most variance in settlement for all three groups: 59% of the model variance for kelp bass, 72% for KGB rockfish, and 78% for OYT rockfish. For all groups, food- and temperature-related variables explained much less variance alone than when interacting with wind or circulation processes. Site-specific effects were important for kelp bass and KGB rockfish but less so for OYT rockfish.

DISCUSSION

The approach we describe here may help to inform fisheries management in several ways. The results of the spatial analysis provide general guidelines as to the scales over which management differences may translate into recruitment variability, by examining the strengths of the links between regional- or basin-level production and/or transport and local recruitment. The spatiotemporal analysis points out the times, places, and conditions that best predicted local settlement over the span of our observations, and thus suggests useful avenues for improved predictive, mechanistic models to forecast year-class strength.

When discussing the results for each species group, we must be explicit about how we interpreted the influence of potential physical drivers acting at different scales of time and space. We assumed that fixed site effects reflected differences among sites in their physical locations

(mainland, island, orientation, windward or leeward) as well as their proximity to persistent or regularly-occurring oceanographic features (e.g., topographically steered flows, stationary fronts, downstream eddies) and other unaccounted-for features such as habitat (e.g., kelp cover, substrate). Although sites differed obviously in the intensity of settlement they received (Fig. 4 and Fig. S2), a surprisingly small amount (4–24%) of the model-explained variance was due to the fixed site effects in the analysis (Fig. 7G–I). We assume that this result reflects that many of the among-site differences related to delivery of organisms can actually be accounted for by local-scale differences in the expression of dynamic bio-physical processes. For simplicity, we discuss the site effect as an indicator of small-scale, site-specific processes. However, because we have not included all possible predictors or spatial scales, it is impossible to say how much of the variance attributed to the fixed site effect might actually be due to a neglected variable operating over any spatial scale smaller than the span of the study sites. Thus the variance attributed to the fixed site effect can alternatively be viewed as a measure of the scope for additional predictors with distinctive spatial patterns to explain model variance. This underscores a subtle but important problem with simple regression approaches to complex spatio-temporal processes (see *Caveats and Future Directions*).

We also note that our analysis considered only effects of forcing factors occurring before settlement. Although postsettlement processes such as predation and competition can clearly have strong and complex regulating effects on populations of marine species, we believe that our use of artificial collectors minimized the influence of such factors. For example, we have previously measured the relationship between settlement to SMURFS, recruitment on reefs, and adult population size for kelp bass in the SBC (White and Caselle, 2008). At the small, within-site scale, both recruitment and adult survivorship of kelp bass were density dependent and

positively related to the abundance of giant kelp (*Macrocystis pyrifera* (L.) C.A. Agardh 1820). At the larger, among-site scale, the spatial pattern of adult kelp bass abundance was predicted well by the pattern of larval supply, but the spatial relationship between giant kelp abundance and kelp bass larval supply was consistently negative despite the positive effects of giant kelp on kelp bass at the smaller spatial scale. We found that the large-scale negative relationship was probably the product of a channel-wide spatial mismatch between oceanographic conditions that favor kelp survival and those that concentrate and distribute fish larvae. The present study builds on our previous work by investigating specific oceanographic conditions that affect settlement in much greater detail and for several species..

Processes associated with delivery

We assume that factors important in the proximal delivery of individuals to sites are those acting at smaller, local scales and shorter time lags. Two studies that measured settlement at short intervals both detected strong correlations between settlement and particular local-scale ocean processes. Findlay and Allen (2002) found that the daily settlement of kelp bass to a single reef at Catalina Island was related positively to tidal amplitude and onshore winds and negatively to SST, all measured daily at the scales of the local reef. They suggested that internal tidal bores were a likely means of onshore transport for kelp bass larvae to the reef. In a study of rockfishes in the Monterey area, A. Ammann (unpubl. data) found that changes in temperature on scales of 2–3 days explained settlement of the same rockfishes studied here; the KGB group settled during times of relaxations in upwelling and warmer waters, and the OYT group during upwelling periods with colder water. One explanation is that the OYT rockfish, with a longer PLD and more developed pelagic juveniles, can withstand periods of offshore flow associated with upwelling and still get back to reefs to settle, unlike the less competent larval stage of the KGB

rockfish. Another explanation is that these groups differ in their exposure to offshore surface flow because of differences in their larval depth distribution (Lenarz et al., 1995). We also found differences between the two rockfish groups in the relative importance of factors acting at local scales and short time lags. Short time-lag measures of offshore wind stress were particularly important at the site scale, accounting for a significant portion of the variance in settlement of the KGB rockfish group, but less so for the OYT group. The OYT rockfish are the only group in this study whose pelagic juveniles have well-developed swimming capabilities, qualities that may lessen their dependence on physical delivery to proper habitat.

In a similar study in central California, Wilson et al. (2008) found no relationship between specific physical events and settlement of either KGB or OYT rockfish. In that study, as in this one, recruitment was measured biweekly, and the authors suggested that a mismatch in scale between the sampling frequency and specific physical events (in this case, event-scale upwelling and relaxation events measured by changes in temperature) obscured significant relationships because the two-week interval between sampling times could encompass multiple upwelling-relaxation cycles (Wilson et al., 2008). Although our data were spatially extensive and long-term, we also measured settlement at biweekly intervals, essentially introducing up to a 14-d lag between settlement and observation. Despite the inability to capture the relationship between settlement and specific event-scale processes (those lasting hours to days), we were able to identify times in the larval life cycle that are important to settlement and determine that groups differed in these times.

Processes Associated with Pelagic Life

In addition to delivery processes, larval survival and transport during the pelagic phase can strongly affect settlement patterns in time and space (Cowen, 2002; Pineda et al., 2007;

Cowen and Sponaugle, 2009). We assumed that these factors were reflected in drivers occurring over larger spatial scales and at time lags corresponding to the pelagic larval/juvenile duration of the species group in question. Note that groups differ in these durations: up to 40 d for kelp bass, 90 d for the KGB rockfishes, and 120 d for the OYT rockfishes.

For both the rockfish groups, factors acting at a regional scale during time lags corresponding to the early larval phase were major contributors to variation in settlement, and these factors generally involved wind and circulation processes rather than food or temperature. In particular, downwelling transport, upwelling pumping, and downwelling pumping at the regional scale, with lags of approximately 2–3 mo, were significant for both groups, although Chl at the regional scale was also important for both groups at lags of ~1–4 mo. This result suggests that transport during the pelagic phase contributes more to successful settlement in these groups than food availability or temperature effects acting alone. Many authors have suggested that year-class strength for rockfishes is set in the larval phase (Ralston and Howard, 1995; Yoklavich et al., 1996; Laidig et al., 2007), although few have separated the effects of wind or circulation affecting transport from those of food availability affecting survival during this phase. Ralston and Howard (1995) found a correlation between rockfish abundance in midwater trawls in the spring and abundance in nearshore surveys in the summer and concluded that year-class strength is set early in the larval phase. VenTresca et al. (1996) found large concentrations of larval rockfishes in January but very few juveniles 3–4 mo later in midwater trawls; they concluded that El Niño conditions in 1992 caused poor survival between the larval and pelagic juvenile stages. Laidig et al. (2007) measured year-class strength with visual SCUBA surveys and performed correlations between an annual index of recruitment and monthly means of ocean parameters with lags and found that all three species measured (blue,

black, and yellowtail rockfishes) were negatively correlated with sea surface anomaly and nearshore temperature in late winter (February–March; the correlations were significant for two out of the three rockfish species during the months of January through May). We provide further evidence that transport and delivery mechanisms, probably in combination with food and/or temperature, are important early in the pelagic phase, not only for rockfishes but for kelp bass as well.

Although our method allows partitioning of explained variance among various processes, note the limitations imposed by the coarse jump in spatial resolution from the ~10-km "local scale" to the >250-km regional and basin scales. In particular, the coarse spatial resolution of our regional analysis of wind/circulation processes, combined with the 8-d resolution of the satellite Chl data, limits our ability to detect and locate mesoscale transient events like blooms, jets, and fronts that might be critical in the period immediately surrounding larval production and release. The greater apparent importance of wind/circulation processes for the rockfish groups does not therefore exclude food availability as a mechanism. Upwelling and primary production along the California coast covary in a definite spatial pattern (Broitman and Kinlan, 2006) that would not be resolved by our 250-km regions. The upwelling indices used here could actually be acting as indices of mesoscale patches of food availability not detected by our spatially and temporally smoothed food-availability proxy (Chl). Future analysis may be able to separate these effects by combining finer spatial- and temporal-scale Chl and SST data with finer spatial-scale wind/circulation estimates in a two-dimensional (rather than along-coast) framework.

The regional scale was most important for all three species groups, perhaps indicating that the sources of fish settlement to the SBC are local, that is, in the SBC itself. Adult population densities of the rockfishes in our study are very low to the south of the SBC, so

rockfish probably come from sources to the north or from the central region itself. Kelp bass populations show the opposite pattern; the likely sources are to the south or in the central region. Some features, including the SBC gyre, may aggregate fish larvae in the SBC; Nishimoto and Washburn (2002) found higher abundances of rockfish larvae inside the gyre, although the effect of larval accumulation on recruitment to reefs in the SBC area remains to be investigated. Regardless of the potential source locations, if larvae aggregate in the channel at early larval stages, then regional oceanography can affect both transport and survival, as suggested by our results.

Kelp bass have the shortest PLD of the three groups we studied, and their settlement was sensitive to processes occurring during the entire larval phase. As with the rockfish, wind and circulation processes, alone and in combination with food and, to a lesser extent, temperature, were important drivers. Their external spawning, pelagic eggs, and small, weakly swimming larvae may make kelp bass more susceptible to the effects of winds, currents, and local food availability than are the rockfishes. Shima and Findlay (2002) found that larval growth rates for kelp bass were a good predictor of juvenile survival and PLD. Slower larval growth resulted in a longer PLD, potentially resulting in higher larval mortality and lower settlement rates. Interestingly, for the kelp bass, the significant forcing factors tended to occur shortly before settlement even at the regional and basin scales. For example, regional downwelling transport and Chl significantly affected kelp-bass settlement at lags <2 weeks. One possibility is that these regional variables are proxies for local-scale effects, which in turn affect delivery of larvae to the nearshore environment.

Processes Associated with Production

Recruitment ultimately depends on production of young, of course, but stock-recruitment relationships are often obscured by the more proximal processes discussed above. We assumed that the influence of production on settlement was reflected in processes that occurred at the sites of production, which could be near or far from the sites of settlement, and at time lags beyond the larval/juvenile pelagic duration for each species group. Although processes occurring at the regional scale and at the longest time lags contributed significantly to variation in settlement for all the species groups, they were relatively more important for the rockfish groups, which, unlike kelp bass, release young only once per year; this detail of life history may strongly link production with recruitment.

Clearly upwelling is important for settlement and recruitment of nearshore organisms in the California current (Norton, 1987; Roughgarden et al., 1988; Farrell et al., 1991; Ainley et al., 1993; Ralston and Howard, 1995; Wing et al., 1995a,b; Bjorkstedt et al., 2002), but taxonomic groups differ in the exact influence of upwelling on settlement. Both the intensity and seasonal variability in upwelling can influence settlement negatively or positively (Larson et al., 1994; A. Ammann, unpubl. data), perhaps through advection or transport away from or toward nearshore areas. A hump-shaped relationship between recruitment and upwelling intensity has been demonstrated for some rockfishes (Norton 1987; Ainley et al., 1993; Ralston and Howard, 1995), which some have interpreted as indicating optimal conditions for larval feeding (Cury and Roy, 1989). In the SBC, where our study took place, the coastline runs east-west, and although upwelling remains an important process, the typical pattern of upwelling-relaxation dynamics observed in the central and northern parts of California (Davis, 1985) is less prominent. Instead, wind-driven and other circulation processes interact with the unique geomorphology of the region to generate a variety of circulation patterns (Harms and Winant, 1998). These may explain

the observed differences between southern California and central and northern California in the importance of local-scale physical processes on the same rockfish groups.

Not surprisingly, factors related to food and temperature (often interacting with wind and circulation) were relatively more important during the production and early larval phases. Regional Chl was significantly related to settlement of the rockfish groups with lags of 1–4 mo, but a major finding of our study was the very strong relative role that wind and circulation play in contributing to variation in settlement. These processes (either alone or interacting with food or temperature) accounted for the majority (up to 78% for the OYT group) of the explained variation, suggesting that transport, delivery, and upwelling are important correlates of settlement success.

In summary, our attempt to partition among spatial and temporal factors the explained variance in settlement of three nearshore fish groups with very different life histories has revealed that the spatial and temporal scales of variation were most similar for the kelp bass and the KGB rockfish group, despite differences in larval duration, size at hatching, size at settlement, and potential swimming abilities. The factors that were most important to these groups occurred at small spatial scales with short lags and larger spatial scales with long lags, indicating that processes affecting final delivery of settlers, pelagic larval life, and production are all important. For the OYT rockfishes, very little variance in settlement was explained by processes occurring at short lags, whereas events occurring during production (and potentially very early larval life) appeared to be relatively more important.

Caveats and Future Directions

Although we were able to estimate the distribution of explained variation across spatial and temporal scales, a substantial amount of variance (40–43%) remained that was not linearly

associated with any of the predictors in the model. Some of this variation may be an inherent property of coastal circulation (Siegel et al., 2008). When wind-driven turbulent eddies are included in circulation models, these eddies appear to accumulate production over time and space, hold larvae together, and deliver them in dense pulses (Siegel et al., 2008; Mitarai et al., in press). This inherent stochasticity would not be easily resolved in analyses such as we conducted. Specifically, it cannot be separated from unexplained variance due to failure to include particular predictors and/or spatiotemporal scales of importance or to our use of a linear prediction framework.

Note that, in our study, temporal lags were continuous, but the spatial scales were fixed at three values (local, regional, and basin). Although this method improves on previous studies that treated time discontinuously (e.g., specifying lags of 1 week or 1 mo; Laidig et al., 2007; Wilson et al., 2008), the next step in this type of analysis will be to vary space in a continuous fashion, sampling oceanographic processes at larger and larger scales. An analysis of this type would provide more detail on the appropriate scales of management and allow more precise identification of the physical and biological oceanographic processes that influence settlement and potentially account for some of the unexplained variance in the present study. To our knowledge, this type of multiscale spatiotemporal analysis has not yet been undertaken for a settlement time series of any marine organism.

Without necessarily leaving the linear regression approach, the present analysis could be improved by inclusion of additional predictors and improvement in the spatial or temporal resolution of the predictor data. The predictors used here (SST, Chl, and winds) are all available at higher spatial and temporal resolution for our study region, but importantly, the present analysis was based only on global, publicly available oceanographic and geographic databases

and could therefore be repeated for virtually any coastal area in the world, regardless of local oceanographic observation infrastructure. In nonupwelling systems, of course, one would want to incorporate some proxy for the dominant nonupwelling ocean-circulation mechanisms, perhaps using geostrophic estimates of flow from sea surface height—also available from standardized, public global satellite oceanographic databases. Additional variables might include actual measures of observed surface and subsurface circulation, nutrients, zooplankton abundance, and other physical, chemical, and biological properties of the ocean, which presumably influence larvae on their journey from source to destination locations along the coast. Data on small-scale (<10-km) variation in habitat near settlement sites might lend mechanistic insight into the variance explained by the fixed site effect in our models.

Linear regression is probably not, however, the most efficient technique for extending the present analysis. The simplicity and accessibility of the linear regression approach is the main reason we have applied it here, yet we have been careful to qualify our results as descriptive and correlative rather and predictive and mechanistic. The cross-validation exercise shows that the model has reasonable predictive power for data from the same sites in the same time domain, but this result is no guarantee that the model could be extended to prediction at other sites or times. We think doing so would be dangerous without a better mechanistic understanding of observed correlations, which is beyond the reach of standard linear-regression techniques. Moreover, considerable effort was required to correct for violations of standard regression assumptions of independence in response and predictor variables. These illustrate some of the reasons ecological studies of factors affecting larval supply must move beyond regression- and ANOVA-based approaches.

Methods are needed that can quantitatively compare mechanistic hypotheses that involve complex interrelationships among variables, including hierarchical structure and nonlinearity. Alternative methods in the regression family include path analysis and structural equation modeling (see, e.g., Price et al., 2005). Spectral (including wavelet) and EOF approaches could also be useful (Bendat and Piersol, 2000), although we think few sets of recruitment data will meet the requirements of these techniques. Perhaps the most promising approach is hierarchical Bayesian estimation, which allows models of arbitrary functional and statistical complexity to be estimated from relatively few data, easily accounts for imbalanced data sets and missing observations, and allows for the incorporation of constraints arising from known structure and dynamics of physical and biological variables of interest (Cressie et al., 2009). Hierarchical Bayesian analysis would also allow estimation of spatial and temporal auto- and cross-correlation of predictor and response variables and identification of optimal integration time and space windows directly within the model. We think this technique is particularly deserving of future research as we move toward a synthetic understanding of the complex, multiscale set of processes influencing larval supply to nearshore fish populations.

ACKNOWLEDGEMENTS

This study could not have been conducted without the help of a large number of divers and "SMURFers," but we especially thank R. J. Barr, M. Sheehy, N. Kashef, D. Stafford, and P. Carlson for their contributions. We thank the California Department of Fish and Game and R. Michalski and M. Kibby for substantial use of the R/V GARIBALDI. The wind data used in this study are from the Research Data Archive (RDA) maintained by the Computational and Information Systems Laboratory at the National Center for Atmospheric Research, sponsored by the National Science Foundation. The original data are available from the RDA (http://dss.ucar.edu) in data set number ds744.4. Funding was provided by the Gordon and Betty Moore Foundation and the David and Lucille Packard Foundation. This is PISCO publication number 330.

LITERATURE CITED

Ainley, D. G., W. J. Sydeman, R. H. Parrish, and W. H. Lenarz. 1993. Oceanic factors influencing distribution of young rockfish (*Sebastes* spp.) in central California: a predator's perspective. CalCOFI Rep. 34: 133–139.

Ammann, A. J. 2004. SMURFs: standard monitoring units for the recruitment of temperate reef fishes. J. Exp. Mar. Biol. Ecol. 299: 135–154.

Anderson, T. W. 1983. Identification and development of nearshore juvenile rockfishes (genus *Sebastes*) in kelp forests off central California. MA thesis, California State Univ., Fresno, California. 216 p.

_____, M. H. Carr, and M. A. Hixon. 2007. Patterns and mechanisms of variable settlement and recruitment of a coral reef damselfish, *Chromis cyanea*. Mar. Ecol. Prog. Ser. 350: 109–116.

Bendat, J. S. and A. G. Piersol. 2000. Random data: analysis and measurement procedures. Third edition. Wiley-Interscience, New York, 594 p.

Bjorkstedt, E. P., L. K. Rosenfeld, B. A. Grantham, Y. Shkedy, and J. Roughgarden. 2002. Distributions of larval rockfishes (*Sebastes* spp.) across nearshore fronts in a coastal upwelling region. Mar. Ecol. Prog. Ser. 242: 215–228.

Broitman, B. R. and B. P. Kinlan. 2006. Spatial scales of benthic and pelagic producer biomass in a coastal upwelling ecosystem. Mar. Ecol. Prog. Ser. 327: 15–25

Carr, M. H. 1991. Habitat selection and recruitment of an assemblage of temperate zone reef fishes. J. Exp. Mar. Biol. Ecol. 146: 113–137.

_____ and C. Syms. 2006. Recruitment. Pages 411–427 *in* L. G. Allen, D. J. Pondella II, and M. H. Horn, eds. The ecology of marine fishes: California and adjacent waters. Univ.

California Press, Berkeley and Los Angeles.

Cressie, N., C. A. Calder, J. S. Clark, J. M. V. Hoef, and C. K. Wikle. 2009. Accounting for uncertainty in ecological analysis: the strengths and limitations of hierarchical statistical modeling. Ecol. Appl. 19: 553–570.

Cowen, R. K. 2002. Larval dispersal and retention and consequences for population connectivity. Pages 149–170 *in* P. F. Sale, ed. Coral reef fishes, dynamics and diversity in a complex ecosystem. Academic Press, San Diego.

_____ and S. Sponaugle. 2009. Larval dispersal and marine population connectivity. Ann. Rev. Mar. Sci. 1: 443–466.

Cury, P. and C. Roy. 1989. Optimal environmental window and pelagic fish recruitment success in upwelling areas. Can. J. Fish. Aquat. Sci. 46: 670–680.

Davis, R. E. 1985. Drifter observations of coastal surface currents during CODE. J. Geophys. Res. 90: 4741–4772.

Deutsch, C. V. and A. G. Journel. 1998. GSLIB: geostatistical software library and user's guide. Oxford Univ. Press, New York, 384 p.

Doherty, P. J., V. Dufour, R. Galzin, M. A. Hixon, M. G. Meekan, and S. Planes. 2004. High mortality during settlement is a population bottleneck for a tropical surgeonfish. Ecology 85: 2422–2428.

Erisman, B. E. and L. G. Allen. 2006. Reproductive behaviour of a temperate serranid fish, *Paralabrax clathratus* (Girard), from Santa Catalina Island, California, U.S.A. J. Fish Biol. 68: 157–184.

Farrell, T. M., D. Bracher, and J. Roughgarden. 1991. Cross-shelf transport causes recruitment to intertidal populations in central California, USA. Limnol. Oceanogr. 36: 279–288.

Findlay, A. M. and L. G. Allen. 2002. Temporal patterns of settlement in the temperate reef fish *Paralabrax clathratus*. Mar. Ecol. Prog. Ser. 238: 237–248.

Fogarty, M. J. and L. W. Botsford. 2007. Population connectivity and spatial management of marine fisheries. Oceanography 20: 112–123.

Gilbert, E. A. 2000. Molecular genetic analysis of temporal recruitment pulses in juvenile kelp rockfish. MA thesis, San Francisco State Univ., San Francisco, California.

_____, R. J. Larson, and J. C. Garza. 2006. Temporal recruitment patterns and gene flow in kelp rockfish (*Sebastes atrovirens*). Mol. Ecol. 15: 3801–3815.

Gunderson, D. R., A. M. Parma, R. Hilborn, J. M. Cope, D. L. Fluharty, M. L. Miller, R.D. Vetter, S. S. Heppell, and H. G. Greene. 2008. The challenge of managing nearshore rocky reef resources. Fisheries 33: 172–179.

Harms, S. and C. D. Winant. 1998. Characteristic patterns of the circulation in the Santa Barbara Channel. J. Geophys. Res. 103: 3041–3065.

Hilborn, R. and C. J. Walters. 1992. Quantitative fisheries stock assessment: choice, dynamics and uncertainty. Chapman and Hall, New York. 570 p.

Laidig, T. E., J. R. Chess, and D. F. Howard. 2007. Relationship between abundance of juvenile rockfishes (*Sebastes* spp.) and environmental variables documented off northern California and potential mechanisms for the covariation. Fish. Bull., U.S., 105: 39–48.

Larson, R. J. 1992. Other nearshore rockfish. Pages 130–131 *in* W. S. Leet, C. M. Dewees, and C. W. Haugen, eds. California's living marine resources and their utilization. California Sea Grant Extension Program, Department of Wildlife and Fisheries Biology, University of California, Davis, California Sea Grant Extension Publication UCSGEP-92-12.

_____, W. H. Lenarz, and S. Ralston. 1994. The distribution of pelagic juvenile rockfish of

the genus *Sebastes* in the upwelling region off central California, California. CalCOFI Rep. 35: 175–221.

Large, W. G., J. C. McWilliams, and S. C. Doney. 1994. Oceanic vertical mixing: a review and a model with a non-local K-profile boundary layer parameterization. Rev. Geophys. 32: 363–403.

Lenarz, W. H., D. A. VenTresca, W. M. Graham, F. B. Schwing, and F. Chavez. 1995. Explorations of El Niño events and associated biological population dynamics off central California. CalCOFI Rep. 36:106–119.

Love, R. M. 1996. Probably more than you want to know about the fishes of the Pacific coast. Really Big Press, Santa Barbara, California. 381 p.

Love, M. S., M. H. Carr, and L. J. Haldorson. 1990. The ecology of substrate-associated juveniles of the genus *Sebastes*. Environ. Biol. Fish. 30: 225–243.

_____, M. Yoklavich, and L. Thorsteinson. 2002. The rockfishes of the northeast Pacific. Univ. California Press, Berkeley and Los Angeles. 404 p.

Miller, D. J. and R. N. Lea. 1972. Guide to the coastal marine fishes of California. Calif. Dep. Fish Game Fish Bull. 157: 1–235.

Milliff, R. F. and J. Morzel. 2001. The global distribution of the time-average wind stress curl from NSCAT. J. Atmos. Sci. 58: 109–131.

Moser, H. G. 1996. Scorpaenidae: scorpionfishes and rockfishes. Pages 733–795 *in* H. G. Moser, ed. The early stages of fishes in the California Current region. CalCOFI Atlas No. 33. Allen Press, Lawrence, Kansas.

Mitarai, S., D. A. Siegel, J. R. Watson, C. Dong, and J. C. McWilliams. (in press). Quantifying connectivity in the coastal ocean with application to the Southern California Bight. J.

Geophys. Res. Oceans.

Nishimoto, M. M. and L. Washburn. 2002. Patterns of coastal eddy circulation and abundance of pelagic juvenile fish in the Santa Barbara Channel, California, USA. Mar. Ecol. Prog. Ser. 241: 183–199.

Norton, S. 1987. Ocean climate influences on groundfish recruitment in the California Current. Pages 73–99 *in* Proceedings of the International Rockfish Symposium, Anchorage, Alaska (Alaska Sea Grant Rep. 87-2), Univ. Alaska, Anchorage.

Oda, D. L., R. J. Lavenberg, and J. M. Rounds. 1993. Reproductive biology of three California species of *Paralabrax* (Pisces: Serranidae). CalCOFI Rep. 34: 122–132.

Pineda, J., J. A. Hare, and S. Sponaugle. 2007. Larval transport and dispersal in the coastal ocean and consequences for population connectivity. Oceanography 20: 22–39.

Price, M. V., N. M. Waser, R. E. Irwin, D. R. Campbell, and A. K. Brody. 2005. Temporal and spatial variation in pollination of a montane herb: a seven-year study. Ecology 86: 2106–2116.

Prince, J. 2003. The barefoot ecologist goes fishing. Fish Fish. 4: 359–371.

Ralston, S. and D. F. Howard. 1995. On the development of year-class strength and cohort variability in two northern California rockfishes. Fish. Bull., U.S., 93: 710–720.

Romero, M. 1988. Life history of the kelp rockfish, *Sebastes atrovirens* (Scorpaenidae). MA Thesis, San Francisco State University, California. 49 p.

Roughgarden, J., S. D. Gaines, and H. Possingham. 1988. Recruitment dynamics in complex life cycles. Science 241: 1460–1466

Sale, P. F., R. K. Cowen, B. S. Danilowicz, G. P. Jones, J. P. Kritzer, K. C. Lindeman, S. Planes, N. V. C. Polunin, G. R. Russ, Y. J. Sadovy and R. S. Steneck. 2005. Critical science gaps

impede use of no-take fishery reserves. Trends Ecol. Evol. 20: 74–80.

Shima, J. S. and A. M. Findlay 2002. Pelagic larval growth rate impacts benthic settlement and survival of a temperate reef fish. Mar. Ecol. Prog. Ser. 235: 303–309.

Siegel, D. A., S. Mitarai, C. J. Costello, S. D. Gaines, B. E. Kendall, R. R. Warner, and K. B. Winters. 2008. Connectivity among nearshore marine populations: the stochastic nature of larval transport. Proc. Natl. Acad. Sci. USA 105: 8974–8979.

Sogard, S. M., E. Gilbert-Horvath, E. C. Anderson, R. Fisher, S. A. Berkeley, and J. C. Garza. 2008. Multiple paternity in viviparous kelp rockfish, *Sebastes atrovirens*. Environ. Biol. Fish. 81: 7–13.

Soluri, E. A. and V. A. Woodson. 1990. World vector shoreline. Int. Hydrogr. Rev. 67: 27–35.

Sponaugle, S., R. K. Cowen, A. Shanks, S. G. Morgan, J. M. Leis, J. Pineda, G. W. Boehlert, M. J. Kingsford, K. Lindeman, C. Grimes, and J. L. Munro. 2002. Predicting self-recruitment in marine populations: biophysical correlates and mechanisms, Bull. Mar. Sci. 70: 341–375.

Steele, M. A., J. C. Malone, A. M. Findlay, M. H. Carr, and G. E. Forrester. 2002. A simple method for estimating larval supply in reef fishes and a preliminary test of limitation of population size by larval supply in the kelp bass, *Paralabrax clathratus*. Mar. Ecol. Prog. Ser. 235: 195–203.

Victor, B. C. 1986. Larval settlement and juvenile mortality in a recruitment-limited coral reef fish population. Ecol. Monogr. 56:145–160

VenTresca, D. A., J. L. Houk, M. J. Paddack, M. L. Gingras, N. L. Crane, and S. D. Short. 1996. Early life-history studies of nearshore rockfishes and lingcod off central California, 1987−92. Cal. Fish Game. Resources Division. Admin. Rep. 96-4. 77 p.

Yoklavich, M. M., V. J. Loeb, M. M. Nishimoto, and B. Daly. 1996. Nearshore assemblages of larval rockfishes and their physical environment off central California during an extended El Niño event 1991–1993. Fish. Bull., U.S., 94: 766–782.

Young, P. H. 1963. The kelp bass (*Paralabrax clathratus*) and its fishery, 1947–1958. Calif. Dep. Fish Game Fish Bull. 122: 1–67.

Warner, R. R. and R. K. Cowen. 2002. Local retention of production in marine populations: evidence, mechanisms, and consequences. Bull. Mar. Sci. 70: 245–249.

White, J. W. and J. E. Caselle. 2008. Scale-dependent changes in the importance of larval supply and habitat to abundance of a reef fish. Ecology 89: 1323–1333.

Wilson J. R., B. R. Broitman, J. E. Caselle, and D. E. Wendt. 2008. Recruitment of coastal fishes and oceanographic variability in central California. Estuarine Coastal Shelf Sci. 79: 483–490.

Wing, S. R., L. W. Botsford, J. L. Largier and L. E. Morgan. 1995a. Spatial structure of relaxation events and crab settlement in the northern California upwelling system. Mar. Ecol. Prog. Ser. 128: 199–211.

_____, J. L. Largier, L. W. Botsford, and J. F. Quinn. 1995b. Settlement and transport of benthic invertebrates in an intermittent upwelling region. Limnol. Oceanogr. 40: 316–329.

ADDRESS: *Marine Science Institute, University of California, Santa Barbara, California 93106.*

Table 1. Regression results for kelp bass, in order of increasing Monte Carlo P-value. Multiple linear regression on response $\log_{10}$(daily settlement rate + 1) with fixed site effect (14 levels), 18 continuous main effects, and all possible second-degree continuous interaction effects (centered).[a,b]

Parameter estimate summary		Main/first effect				Second effect			
Sign[c]	P-value[d]	Effect[e]	Scale	Process	Time[f]	Effect[e]	Scale	Process	Time[f]
					Fixed effect				
n/a	0*	Site	Site	Site	0, 0	—	—	—	—
					Main effects				
–	0.007*	Downwelling transport, central	Region	Wind/Circ	5, –3	—	—	—	—
–	0.012*	Chlorophyll, south	Basin	Food	15, –7	—	—	—	—
+	0.035	Upwelling transport, south	Basin	Wind/Circ	15, –13	—	—	—	—

–	0.046	Ekman transport, north	Basin	Wind/Circ	15, –2	—	—	—	—
+	0.047	SST, south	Basin	Temp	15, –22	—	—	—	—
				Interactions					
+	0.006*	SST, site	Local	Temp	5, –6	Downwelling pumping, north	Basin	Wind/Circ	5, –124
–	0.008*	Chlorophyll, central	Region	Food	30, –124	Chlorophyll, south	Basin	Food	15, –7
+	0.015	Downwelling transport, central	Region	Wind/Circ	5, –3	Upwelling transport, south	Basin	Wind/Circ	15, –13
–	0.016	Downwelling transport, central	Region	Wind/Circ	5, –3	Downwelling pumping, south	Basin	Wind/Circ	5, –3
–	0.016	Downwelling pumping, central	Region	Wind/Circ	5, –6	Downwelling pumping, south	Basin	Wind/Circ	5, –3
–	0.021	Downwelling transport, central	Region	Wind/Circ	5, –3	Chlorophyll, south	Basin	Food	15, –7
–	0.024	Chlorophyll, central	Region	Food	4, –2	SST, site	Local	Temp	5, –6

–	0.032	Chlorophyll, central	Region	Food	30, –124	Chlorophyll, north	Basin	Food	15, –83
–	0.038	Chlorophyll, central	Region	Food	4, –2	Offshore wind stress, site	Local	Wind/Circ	1, –6
–	0.043	Chlorophyll, south	Basin	Food	15, –7	Downwelling pumping, south	Basin	Wind/Circ	5, –3

[a]This table includes only effects with Monte Carlo P-values <0.05. These P-values are reported without correction for multiple testing. Those marked with asterisks were also significant in cross-validation; that is, the 95% confidence interval (CI) for the parameter estimate under cross-validation lay completely above the Monte Carlo 95% CI under the simulated null hypothesis.

[b]Whole-model statistics: N = 1068; model d.f. = 184; error d.f. = 883; F-ratio = 6.49 (Monte Carlo P < 0.0001); R^2 = 0.57 (Monte Carlo P < 0.0001, bootstrap 95% CI: 0.56, 0.60); cross-validation R^2 = 0.29 (95% CI: 0.09, 0.51).

[c]Sign of the estimated coefficient for this term (not applicable for fixed site effect).

[d]Monte Carlo P-value for the simulated effect test.

[e]"North," "central," and "south" refer to the three regions illustrated in Figure 2B.

[f]Time window followed by time lag.

Table 2. Regression results for the KGB species group (the kelp, gopher, and black-and-yellow rockfishes). Multiple linear regression on response $\log_{10}$(daily settlement rate + 1) with fixed site effect (14 levels), 13 continuous main effects, and all possible second-degree continuous interaction effects (centered). Column headings as in Table 1.[a,b]

Parameter estimate summary		Main/first effect				Second effect			
Sign	P-value	Effect	Scale	Process	Time	Effect	Scale	Process	Time
				Fixed effect					
n/a	0.010*	Site	Site	Site	0, 0	—	—	—	—
				Main effect					
+	0.013*	Offshore wind stress, site	Local	Wind/Circ	1, –6	—	—	—	—
				Interaction effects					
+	0.013*	Chlorophyll, central	Region	Food	30, –115	Downwelling transport, central	Region	Wind/Circ	15, –110

–	0.016	Downwelling pumping, central	Region	Wind/Circ	15, –50	Downwelling Pumping, north	Basin	Wind/Circ	15, –30
+	0.022	Ekman transport, central	Region	Wind/Circ	30, –55	Downwelling transport, central	Region	Wind/Circ	15, –110
+	0.022	Ekman transport, central	Region	Wind/Circ	30, –55	Chlorophyll, south	Basin	Food	4, –30
+	0.024	Ekman transport, central	Region	Wind/Circ	30, –55	Offshore wind stress, site	Local	Wind/Circ	1, –6
–	0.030	Downwelling pumping, central	Region	Wind/Circ	15, –50	Chlorophyll, south	Basin	Food	4, –30
–	0.037	SST, central	Region	Temp	30, –25	Downwelling transport, central	Region	Wind/Circ	15, –110
–	0.047	Ekman pumping, site	Local	Wind/Circ	1, –7	Offshore wind stress, site	Local	Wind/Circ	1, –6
–	0.048	SST, central	Region	Temp	30, –25	Downwelling pumping, central	Region	Wind/Circ	15, –50

–	0.048	Ekman pumping, site	Local	Wind/Circ 1, –7	Downwelling pumping, south	Basin	Wind/Circ	15, –110	

[a]This table includes only effects with Monte Carlo P-values <0.05. These P-values are reported without correction for multiple testing. Those marked with asterisks were also significant in cross-validation; that is, the 95% confidence interval (CI) for the parameter estimate under cross-validation lay completely above the Monte Carlo 95% CI under the simulated null hypothesis.

[b]Whole-model statistics: N = 1068; model d.f. = 104; error d.f. = 963; F-ratio = 13.699 (Monte Carlo P < 0.0001); R^2 = 0.60 (Monte Carlo P < 0.0001, bootstrap 95% CI: 0.57, 0.63); cross-validation R^2 = 0.29 (95% CI: 0.09, 0.68).

Table 3. Regression results for the OYT species group (the olive and yellowtail rockfishes). Multiple linear regression on response $\log_{10}$(daily settlement rate + 1) with fixed site effect (14 levels), 17 continuous main effects, and all possible second-degree continuous interaction effects (centered). Column headings as in Table 1.[a,b]

Parameter estimate summary		Main/first effect				Second effect			
Sign	P-value	Effect	Scale	Process	Time	Effect	Scale	Process	Time
					Main effects				
–	0.002*	Chlorophyll, central	Region	Food	30, –101	—	—	—	—
+	0.004	Ekman pumping, site	Local	Wind/Circ	1, –12	—	—	—	—
+	0.014	SST, central	Region	Temp	15, –6	—	—	—	—
–	0.017	SST, site	Local	Temp	5, –29	—	—	—	—
+	0.031	Chlorophyll, central	Region	Food	4, –39	—	—	—	—
					Interactions				

+	0.001*	Ekman pumping, site	Local	Wind/Circ	1, –12	Downwelling pumping, north	Basin	Wind/Circ	15, –15
–	0.004	Chlorophyll, central	Region	Food	30, –101	Downwelling pumping, north	Basin	Wind/Circ	15, –15
–	0.005	Downwelling pumping, central	Region	Wind/Circ	15, –46	Ekman transport, south	Basin	Wind/Circ	15, –18
–	0.005	Downwelling pumping, south	Basin	Wind/Circ	15, –91	Downwelling pumping, north	Basin	Wind/Circ	15, –15
+	0.006	Ekman transport, central	Region	Wind/Circ	15, –54	Ekman transport, south	Basin	Wind/Circ	15, –18
+	0.023	Ekman transport, site	Local	Wind/Circ	3, –1	Ekman transport, north	Basin	Wind/Circ	15, –2
–	0.033	SST, site	Local	Temp	5, –29	Downwelling pumping, north	Basin	Wind/Circ	15, –15
–	0.034	Chlorophyll, central	Region	Food	30, –101	Downwelling transport, central	Region	Wind/Circ	15, –98

–	0.037	Ekman transport, central	Region	Wind/Circ	15, –54	SST, site	Local	Temp	5, –29
+	0.04	SST, central	Region	Temp	15, –6	Downwelling transport, central	Region	Wind/Circ	15, –98
+	0.048	SST, site	Local	Temp	5, –29	Downwelling pumping, central	Region	Wind/Circ	15, –46
+	0.049	Downwelling transport, central	Region	Wind/Circ	15, –98	Chlorophyll, north	Basin	Food	4, –15

[a]This table includes only effects with Monte Carlo P-values <0.05. These P-values are reported without correction for multiple testing. Those marked with asterisks were also significant in cross-validation; that is, the 95% confidence interval (CI) for the parameter estimate under cross-validation lay completely above the Monte Carlo 95% CI under the simulated null hypothesis.

[b]Whole-model statistics: N = 1068; model d.f. = 166; error d.f. = 901; F-ratio = 8.26 (Monte Carlo P < 0.0001); R^2 = 0.60 (Monte Carlo P < 0.0001, bootstrap 95% CI: 0.56, 0.67); cross-validation R^2 = 0.24 (95% CI: 0, 0.74)

APPENDIX

Potential predictor set. Indices, derived from oceanographic databases of satellite-derived observations, of wind-driven circulation, surface temperature, and surface chlorophyll concentration at various spatial scales ("spatial integration window") and distances from the settlement sampling sites ("spatial lag"). North, central, and south regions are illustrated in Fig. 2B.

Short name	Full name	Description	Units	Transform[a]	Spatial scale[b]	Window (km)[c]	Lag (km)[d]
Site	Fixed site effect	Unexplained site-to-site differences	none	none	Site	1	0
Local Ekman transport	Ekman transport near site (positive values correspond to upwelling)	Magnitude of theoretical offshore volume transport due to Ekman transport driven by the observed alongshore component of the wind stress; alongshore is defined according to the average coastline orientation (azimuth angle) in a 10-km window centered on the site of interest	$m^3 \cdot s^{-1} \cdot m$ $coast^{-1}$	none	Site	10	0

Local Ekman pumping	Ekman pumping near site (positive values correspond to upwelling)	Magnitude of theoretical offshore volume transport that would occur as a result of Ekman pumping driven by the observed curl of the wind stress, integrated along a 10-km cross-shore transect	$m^3 \cdot s^{-1} \cdot m$ $transect^{-1}$	none	Site	10	0
Local SST	Daily mean satellite sea surface temperature (SST) in 12- × 12-km rectangle centered on site	Mean SST in 3- × 3-pixel (12- × 12-km) rectangle centered on site, from Pathfinder v5.0 AVHRR SST, average of night and day 5-d composites, linearly interpolated to daily interval	°C	none	Site	12	0

Local offshore wind stress	Offshore wind stress near site (positive values correspond to onshore flow)	Magnitude of offshore wind stress in vicinity of site	$N \cdot m^{-2}$	none	Site	10	0
Chlorophyll, central	Surface chlorophyll-*a* concentration in central region	SeaWiFS 8-d, 4-km surface chlorophyll-*a* concentration, averaged over region and interpolated to daily time interval	$mg \cdot m^{-3}$	$\log_{10}(x+1)$	Region	250	0
Downwelling pumping, central	Total downwelling pumping in central region (spatially integrated)	Downwelling due to Ekman pumping summed over region	$\sum(m^3 \cdot s^{-1} \cdot m\ transect^{-1})$	$\sqrt{(x+1)}$	Region	250	0

Downwelling transport, central	Same as previous, central region	Downwelling due to Ekman transport summed over region	$\sum(m^3 \cdot s^{-1} \cdot m\ coast^{-1})$	$\sqrt{(x+1)}$	Region	250	0
Upwelling pumping, central	Total upwelling pumping in central region (spatially integrated)	Upwelling due to Ekman pumping summed over region	$\sum(m^3 \cdot s^{-1} \cdot m\ transect^{-1})$	$\sqrt{(x+1)}$	Region	250	0
Upwelling transport, central	Same as previous, central region	Upwelling due to Ekman transport summed over region	$\sum(m^3 \cdot s^{-1} \cdot m\ coast^{-1})$	$\sqrt{(x+1)}$	Region	250	0

Ekman transport, central	Ekman transport in central region (positive values correspond to upwelling)	Magnitude of theoretical offshore volume transport due to Ekman transport driven by the observed alongshore component of the wind stress; alongshore is defined as above but in a 100-km	$m^3 \cdot s^{-1} \cdot m$ coast^{-1}	none	Region	250	0
Ekman pumping, central	Ekman pumping in central region (positive values correspond to upwelling)	Magnitude of theoretical offshore volume transport that would occur as a result of Ekman pumping driven by the observed curl of the wind stress, integrated along a 10-km cross-shore transect.	$m^3 \cdot s^{-1} \cdot m$ coast^{-1}	none	Region	250	0
SST, central	Spatial average of satellite SST in central region	Pathfinder v5.0 AVHRR satellite SST, 5-d, 4-km product, averaged over region and interpolated to daily time interval	°C	none	Region	250	0

Chlorophyll, north	Surface chlorophyll concentration in north region	SeaWiFS Chl-*a* 8-d, 4-km product, averaged over region and interpolated to daily time interval	$mg \cdot m^{-3}$	$\log_{10}(x+1)$	Basin	250	-200
Chlorophyll, south	Surface chlorophyll concentration in south region	Same as previous, south region	$mg \cdot m^{-3}$	$\log_{10}(x+1)$	Basin	250	200
Downwelling pumping, north	Total downwelling pumping in north region (spatially integrated)	Downwelling due to Ekman pumping summed over region	$\sum(m^3 \cdot s^{-1} \cdot m\ transect^{-1})$	$\sqrt{(x+1)}$	Basin	250	-200

Downwelling pumping, south	Same as previous, south region	Downwelling due to Ekman pumping summed over region	$\sum(m^3 \cdot s^{-1} \cdot m\ transect^{-1})$	$\sqrt{(x+1)}$	Basin	250	200
Upwelling transport, north	Total upwelling transport in north region (spatially integrated)	Upwelling due to Ekman transport summed over region	$\sum(m^3 \cdot s^{-1} \cdot m\ coast^{-1})$	$\sqrt{(x+1)}$	Basin	250	-200
Upwelling transport, south	Same as previous, south region	Upwelling due to Ekman transport summed over region	$\sum(m^3 \cdot s^{-1} \cdot m\ coast^{-1})$	$\sqrt{(x+1)}$	Basin	250	200

Ekman transport, north	Ekman transport in north region (positive values correspond to upwelling)	Magnitude of theoretical offshore volume transport due to Ekman transport driven by the observed alongshore component of the wind stress, alongshore is defined as above, in a 100-km window	$m^3 \cdot s^{-1} \cdot m\ coast^{-1}$	none	Basin	250	-200
Ekman transport, south	Same as previous, south region	Same as previous, south region	$m^3 \cdot s^{-1} \cdot m\ coast^{-1}$	none	Basin	250	200
SST, south	Spatial average of satellite SST in south	Pathfinder v5.0 AVHRR satellite SST 5-d, 4-km product, averaged over region and interpolated to daily time interval	°C	none	Basin	250	200

[a]The function used to transform data for approximate normality and homogeneity of variances before correlation and regression analyses.

[b]Site, region, and basin scales are described in Figure 2B.

[c]Spatial integration window (km); approximate, based on latitudinal bounds that defined regions of interest (Fig. 2B).

[d]Spatial lab; approximate, based on latitudinal bounds that defined regions of interest (Fig. 2B).

FIGURE LEGENDS

Figure 1. Conceptual model of processes that may affect recruitment of the species complexes we studied. Timing in this example is for the kelp bass (*Paralabrax clathratus*).

Figure 2. (A) Study sites in the Santa Barbara Channel. Site locations are indicated by black dots; see Table S1 for other site characteristics. Coastline is shown by heavy black line, light black lines indicate depth contours in meters. (B) Map showing central region (containing study sites from A) and regions of similar latitudinal and offshore extent shifted to the north and south of the central region, where time- and space-lagged physical drivers may act to affect settlement in the central region. Correlations between processes measured in the central region and settlement at study sites are defined as "regional scale." Correlations between processes measured in the north or south region and settlement at study sites are defined as "basin scale."

Figure 3. Regional potential biophysical driver time series. (A, B, C) Sea surface temperature in north, central, and south regions. (D, E, F) Surface chlorophyll-*a* concentration in north, central, and south regions. (G, H, I) Ekman transport in north, central, and south regions. (J, K, L) Ekman pumping in north, central, and south regions. In panels G through L, values >0 (above the dashed horizontal reference line) indicate upwelling, and those <0 indicate downwelling. Each regional physical variable is described in detail in Table S1 and the Appendix.

Figure 4. Time series of settlement and local-scale potential physical drivers. Shown here is an example for site 6 (the westernmost site on the north shore of Santa Cruz Island, the

largest of the islands in Fig. 1A). Similar plots for all other sites are given in Figure S2A–N. Lower axis: daily settlement rate time series for kelp bass (KB, x's); the kelp, gopher, and black-and-yellow rockfishes (KGB, open circles); and the olive and yellowtail rockfishes (OYT, filled circles) at this site. Note that daily settlement rate values have been scaled differently for the different species groups, as indicated by vertical axis labels. Upper four axes: local-scale potential physical driver time series in the vicinity of the site (spatial resolution was approximately 10–12 km). For each physical time series, to facilitate among-site comparisons, labels on the vertical axis show the grand mean of the variable (pooled for all sites), plus and minus two standard deviations of the pooled data. Each local physical variable is described in detail in Table S1 and the Appendix. Positive values of Ekman pumping and Ekman transport indicate upwelling. Positive values of offshore-onshore wind stress indicate onshore wind flow. SST, sea surface temperature.

Figure 5. QuikSCAT/NCEP blended winds and derived indices of Ekman transport and pumping for the central (Santa Barbara Channel) region. (A) Average wind vector field, leading to (B) the corresponding theoretical Ekman transport at the coast (indicated by shading). (C) Average curl of the wind stress, leading to (D) the corresponding theoretical volume transport due to Ekman pumping integrated along a hypothetical shore-normal transect *L* of length 100 km for each coastal location. Diagram on coastline of (A) shows example determination of along-shore and cross-shore directions from the average coastline orientation calculated in a 100-km window centered on a point on the coast (orientation of island sites were determined with a 10-km window; all orientations are given in Table S1). Diagram on coastline of (C) shows hypothetical transect *L*

(dashed line) over which Ekman pumping would be integrated to yield a measure of pumping (in units equivalent to those of Ekman transport) associated with this point on the coast.

Figure 6. Examples of identification of peak lags from (driver, response) cross-correlation functions. Cross-correlations are plotted in dashed grey and solid black lines. Solid black portions of plotted lines are significant at the $P < 0.05$ level (two-tailed *t*-test, uncorrected for multiple testing). Data were smoothed with a rectangular moving-average filter ("integration window") before correlation analysis. Choice of window size(s) was based on preliminary examination of cross-correlation plots of unsmoothed data series. Driver and response variable names are indicated with each panel. Potential drivers considered were (bio)physical time series, transformed for normality as described in the Appendix. Responses were log10(x + 1)-transformed recruitment (daily settlement rate) time series. The integration windows and peak lags chosen for the examples given here were (A) window = 30 d, lag = –55 d; (B) window = 15 d, lag = –2 d; (C) window = 5 d, lag = –15 d; and (D) window = 5 d, lag = –3 d.

Figure 7. Space, time and process for the three species groupings. Columns are species groups (as in Fig. 4), and rows are space (A, B, C), time (D, E, F), and process (G, H, I). Error bars show bootstrap 95% confidence intervals (CI) for variance fractions. Asterisks above bars indicate variance fractions that were significantly larger than expected under the null hypothesis based on Monte Carlo simulation (*$P < 0.05$, **$P < 0.01$, ***$P < 0.001$). Approximate spatial scales: Site, 0 to <10 km; Local, 10–12 km; Region, 250 km; Basin, 500–750 km. For space, bars show the average of sum-of-squares and hierarchical-model-comparison methods of calculating the variance fraction, and CI are

the larger of the bootstrap 95% CI and the standard deviation of the results from the two alternative methods of calculation. Circ, Circulation; Temp, Temperature.

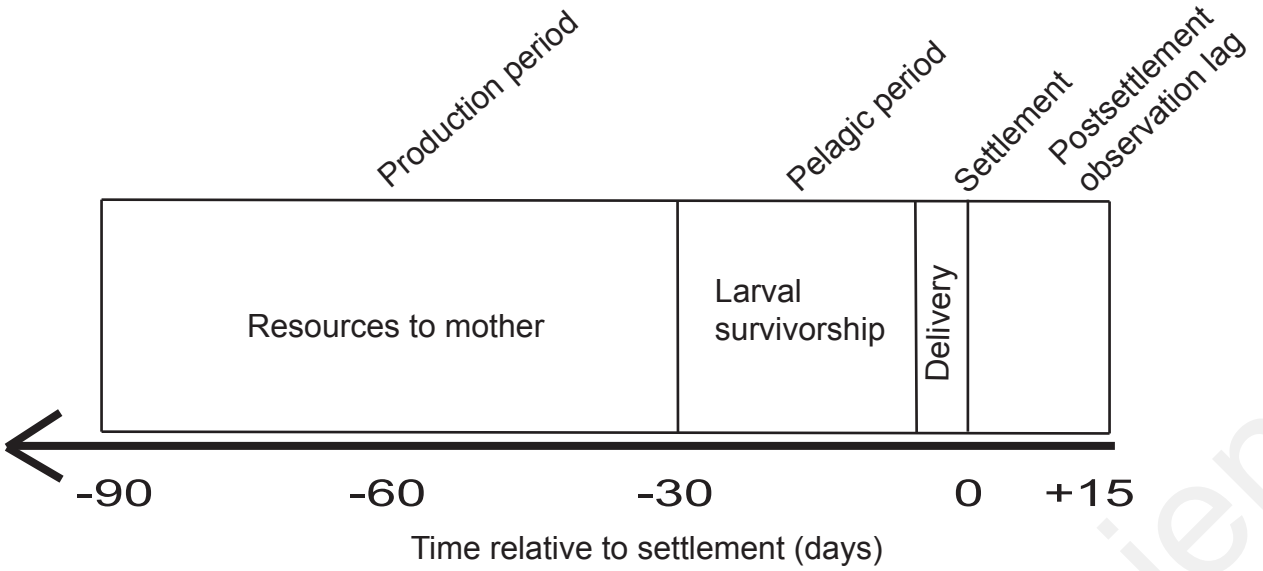

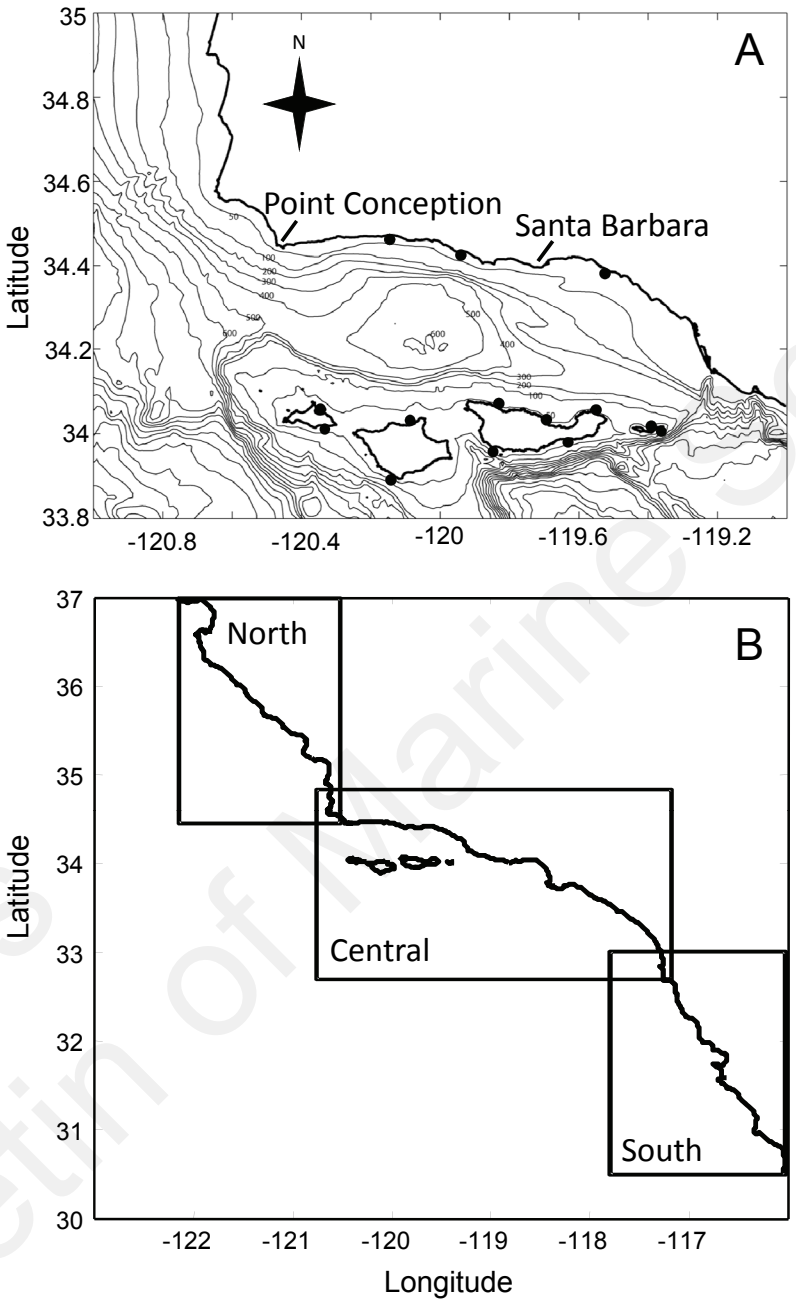

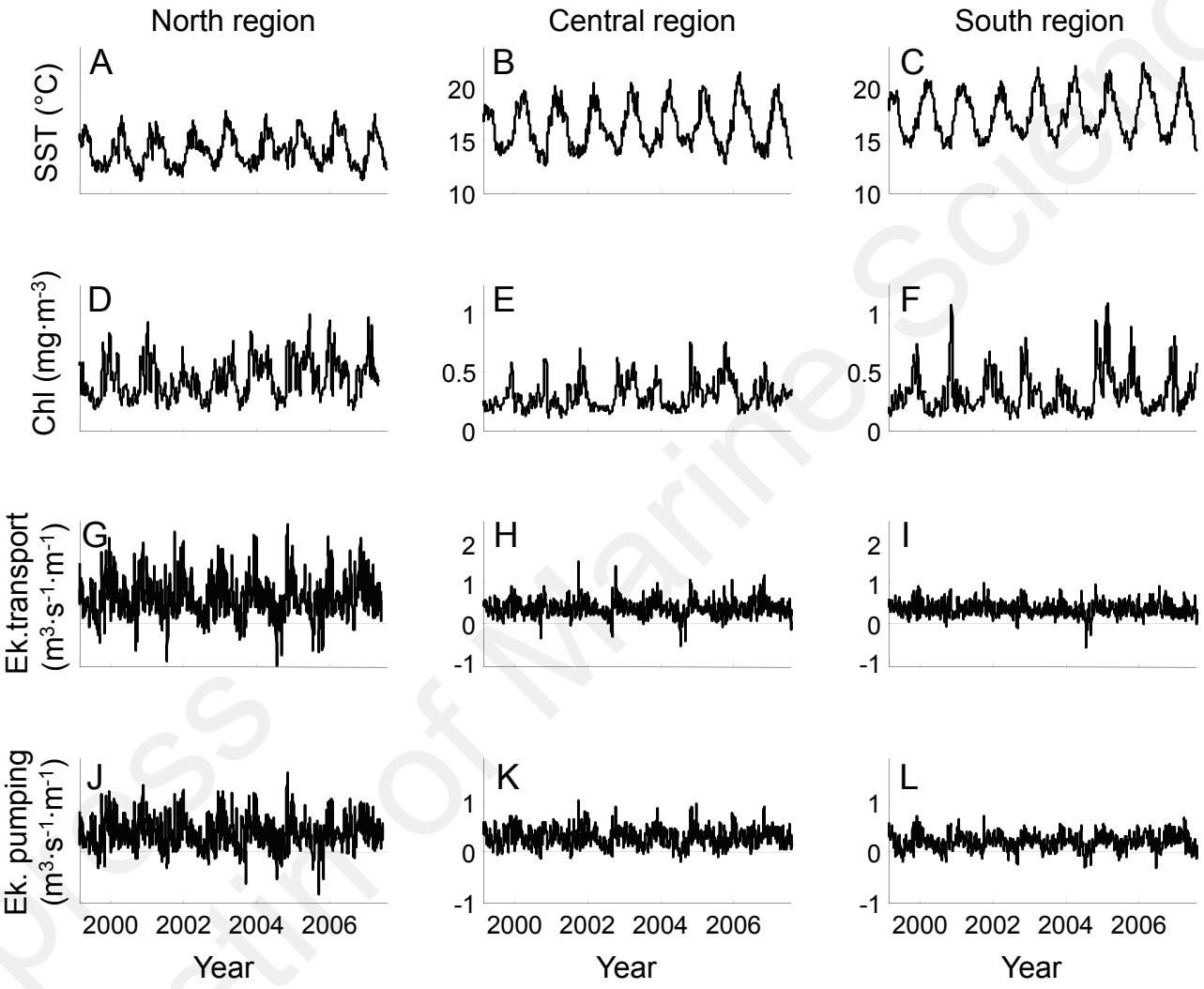

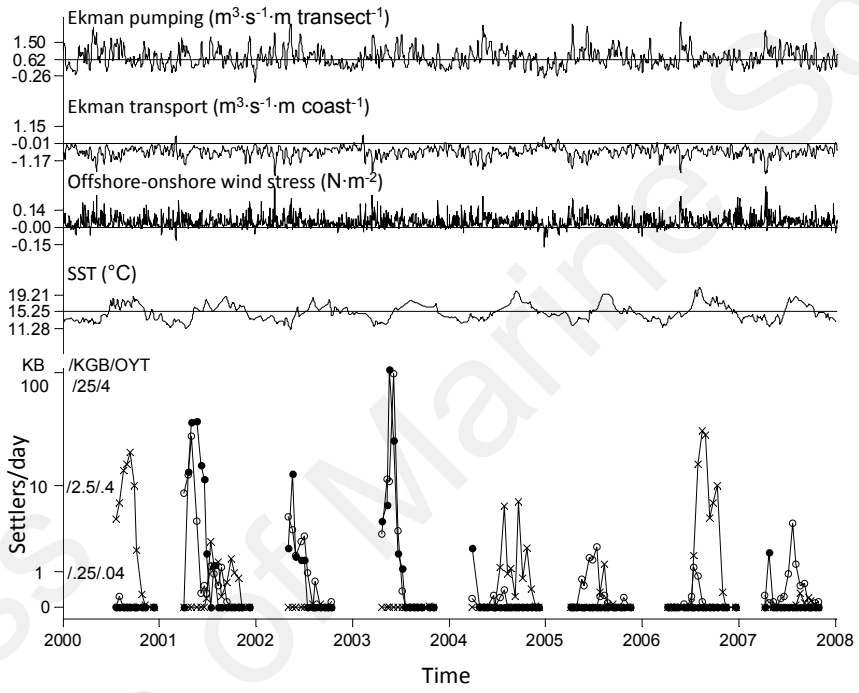

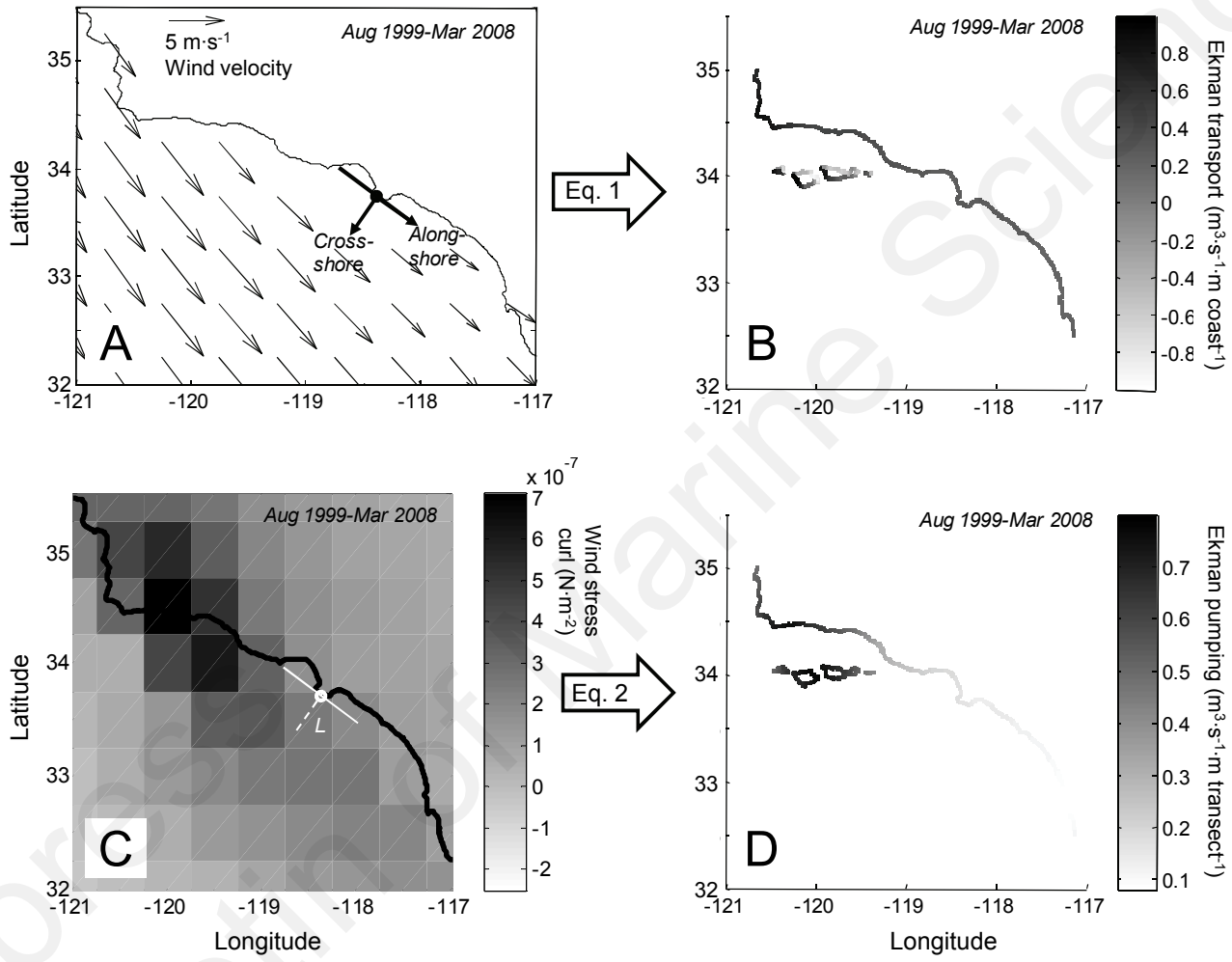

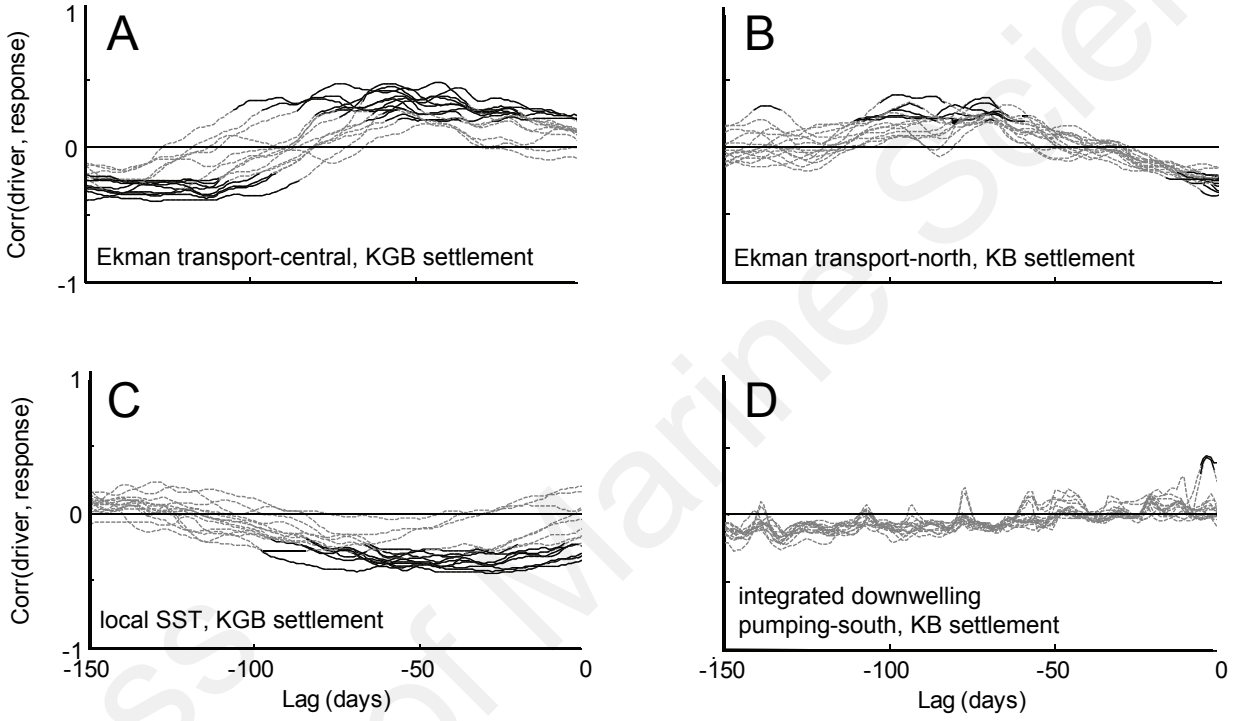

Table S1. Characteristics of the 14 sites in the Santa Barbara Channel at which larval fish settlement was sampled for our study. Azimuth angle is the coastline orientation measured in degrees clockwise from north, calculated in 10, 50, and 100 km neighborhoods around the site. Average oceanography is the time-averaged value of each local oceanographic variable described in the Appendix: SST, sea surface temperature, °C; τ_{off}, local offshore wind stress, $N \cdot m^{-2}$; M_t, local Ekman transport, $m^3 \cdot s^{-1} \cdot m\ coast^{-1}$; M_p, local Ekman pumping, $m^3 \cdot s^{-1} \cdot m\ transect^{-1}$. Average settlement rate is the average number of individuals settling per day on artificial collectors at each site. KB, kelp bass; KGB, the kelp, gopher, and black-and-yellow rockfishes; OYT, and the olive rockfish and yellowtail rockfish.

Site no.	Latitude	Longitude	Start	Azimuth angle, degrees			Average oceanography				Average settlement rate		
	(degrees)	(degrees)	year	10 km	50 km	100 km	SST	τ_{off}	M_t	M_p	KB	KGB	OYT
1	34.0109	–119.3683	2000	311			15.9	0.01	–0.48	0.42	0.5628	0.0309	0.0000
2	34.0083	–119.3957	2002	264			15.9	0.03	–0.29	0.44	1.1316	0.0611	0.0006
3	34.4665	–120.1319	2003	97	95	100	15.1	–0.05	0.53	0.70	0.0195	0.0256	0.0032
4	34.3889	–119.5410	2003	118	109	116	15.5	–0.02	0.43	0.47	0.0861	0.0460	0.0131
5	34.4261	–119.9330	2001	114	100	96	15.2	–0.04	0.44	0.63	0.0781	0.0027	0.0000
6	34.0610	–119.8291	2000	285	259		15.0	0.04	–0.59	0.70	1.7520	0.4796	0.0498
7	33.9662	–119.8538	2005	110	112		15.5	–0.04	0.68	0.74	0.2448	0.0413	0.0000
8	34.0314	–119.6976	2000	296	277		15.6	0.03	–0.61	0.64	2.0568	0.2319	0.0559
9	34.0525	–119.5579	2003	273	321		15.7	0.04	–0.39	0.54	0.3676	0.0850	0.0044
10	34.0623	–120.3559	2003	273			14.3	0.07	–0.59	0.63	0.0222	0.4301	0.0151
11	34.0159	–120.3316	2003	77			14.4	–0.08	0.36	0.63	0.0091	0.0728	0.0216
12	34.0247	–120.0818	2003	269			14.5	0.06	–0.51	0.78	0.0886	0.0648	0.0083
13	33.8961	–120.1282	2003	90			15.1	–0.07	0.57	0.68	0.0121	0.0783	0.0029
14	33.9828	–119.6626	2003	77	74		15.8	–0.05	0.29	0.63	0.2650	0.0701	0.0042

Table S2. Number of sample collections per site per year. Start date and end date (month/day) of sampling in each year. Note that not all sites started or ended on the same day.

Site	2000	2001	2002	2003	2004	2005	2006	2007
1	8	16	11	14	18	15	16	15
2	—	—	11	14	18	15	16	15
3	—	—	—	15	17	14	14	12
4	—	—	—	15	17	15	15	13
5	—	6	—	—	10	14	14	13
6	10	17	12	13	17	16	17	15
7	—	—	—	—	—	13	16	14
8	10	17	12	13	17	15	17	15
9	—	—	—	13	18	14	16	15
10	—	—	—	12	14	12	11	10
11	—	—	—	12	14	12	10	10
12	—	—	—	11	14	12	11	10
13	—	—	—	11	13	12	10	11
14	—	—	—	14	18	15	16	15
First collection date	07/21	04/04	05/02	04/09	03/29	03/30	04/07	04/09
Last collection date	12/12	12/07	10/17	11/06	12/09	11/16	12/20	11/02

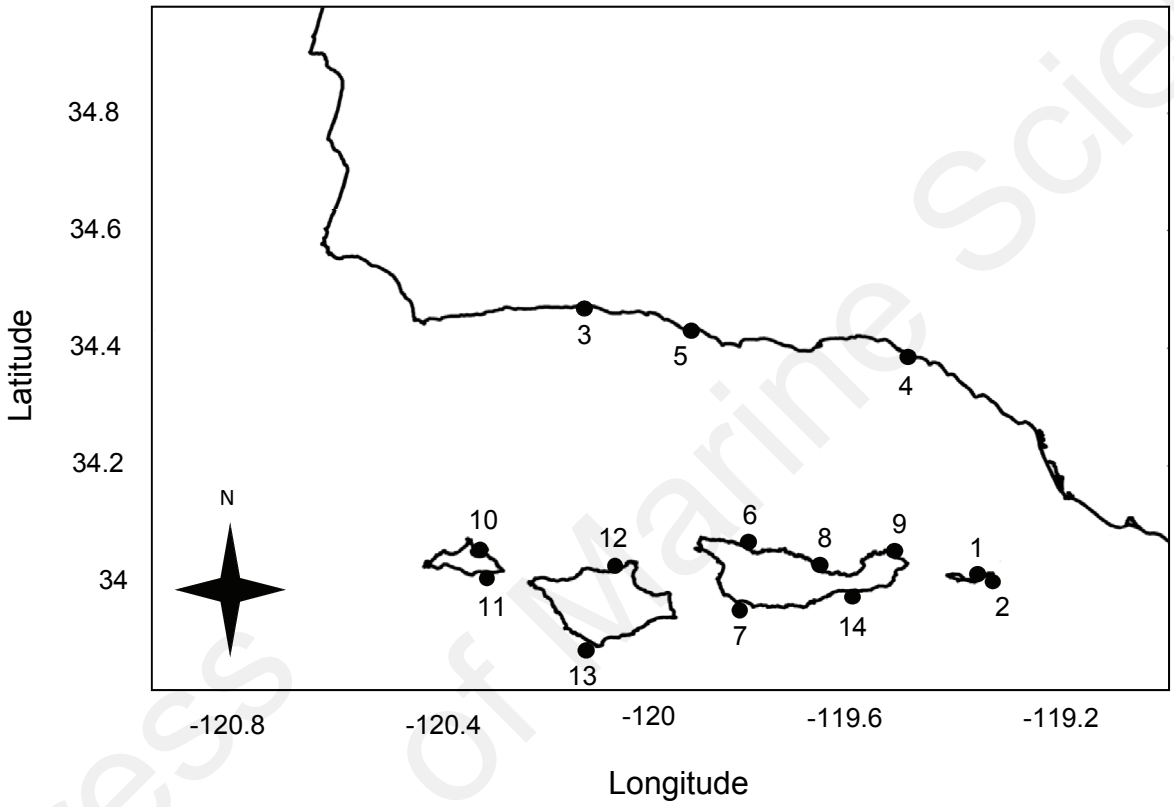

Figure S1. Map of study sites showing site numbers corresponding to those used in Table S1 and Figure S2.

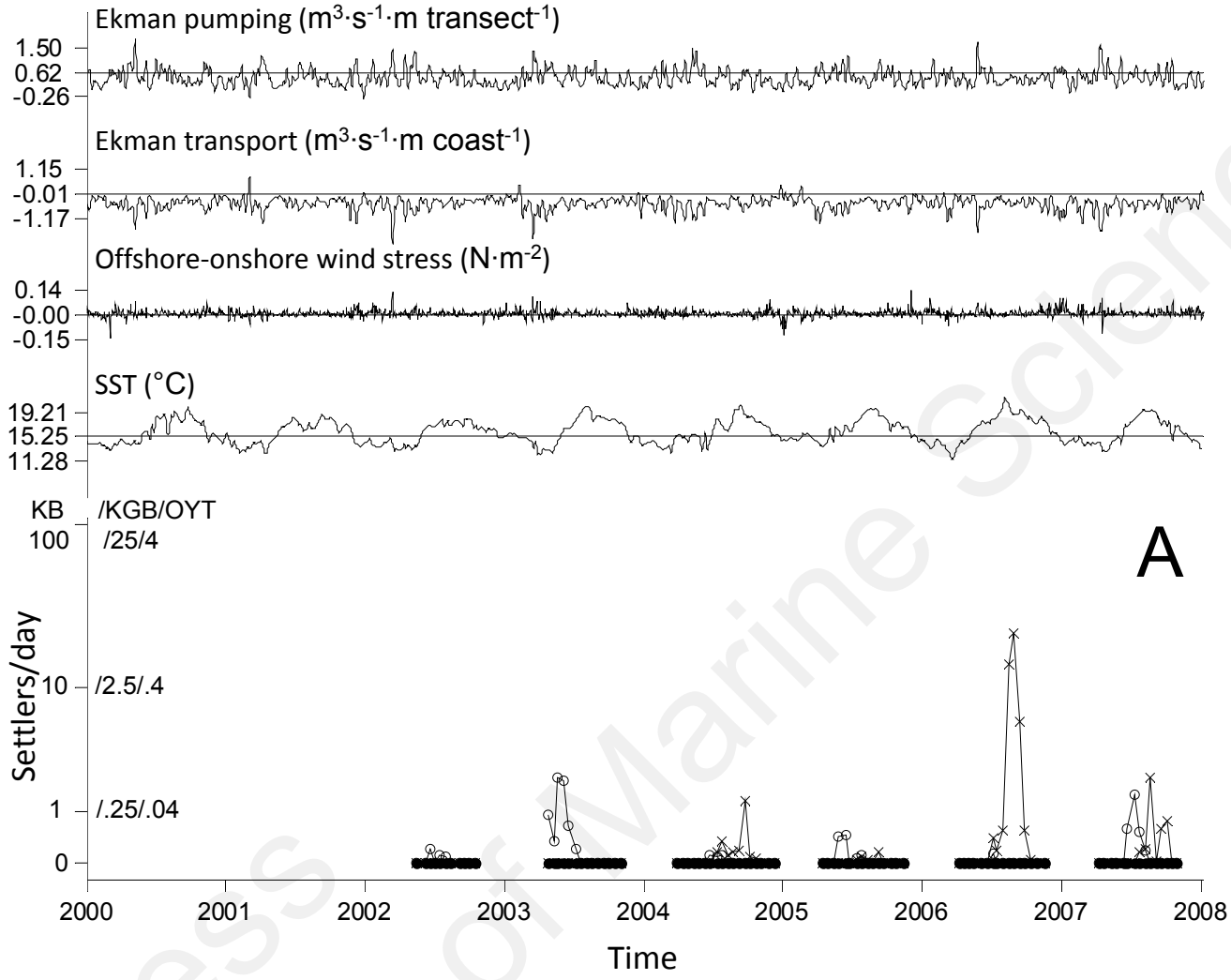

Figure S2. (A) Time series of settlement and local-scale potential physical drivers for site 1 (see Table S1 for all site numbers and characteristics). Lower axis: daily settlement rate time series for kelp bass (KB, x's), the kelp, gopher, and black-and-yellow rockfishes (KGB, open circles), and the olive rockfish and yellowtail rockfishes (OYT, filled circles) at this site. Note that daily settlement rate values have been scaled differently for the different species groups, as indicated by vertical axis labels. Upper four axes: local-scale potential physical driver time series in the vicinity of the site (spatial resolution was approximately 10–12 km). For each physical time series, to facilitate among-site comparisons, labels on the vertical axis show the grand mean of the variable (pooled for all sites), plus and minus two standard deviations of the pooled data. Each physical variable is described in detail in Table S1 and the Appendix. Positive values of Ekman pumping and Ekman transport indicate upwelling. Positive values of offshore-onshore wind stress indicate onshore wind flow. SST, sea surface temperature.

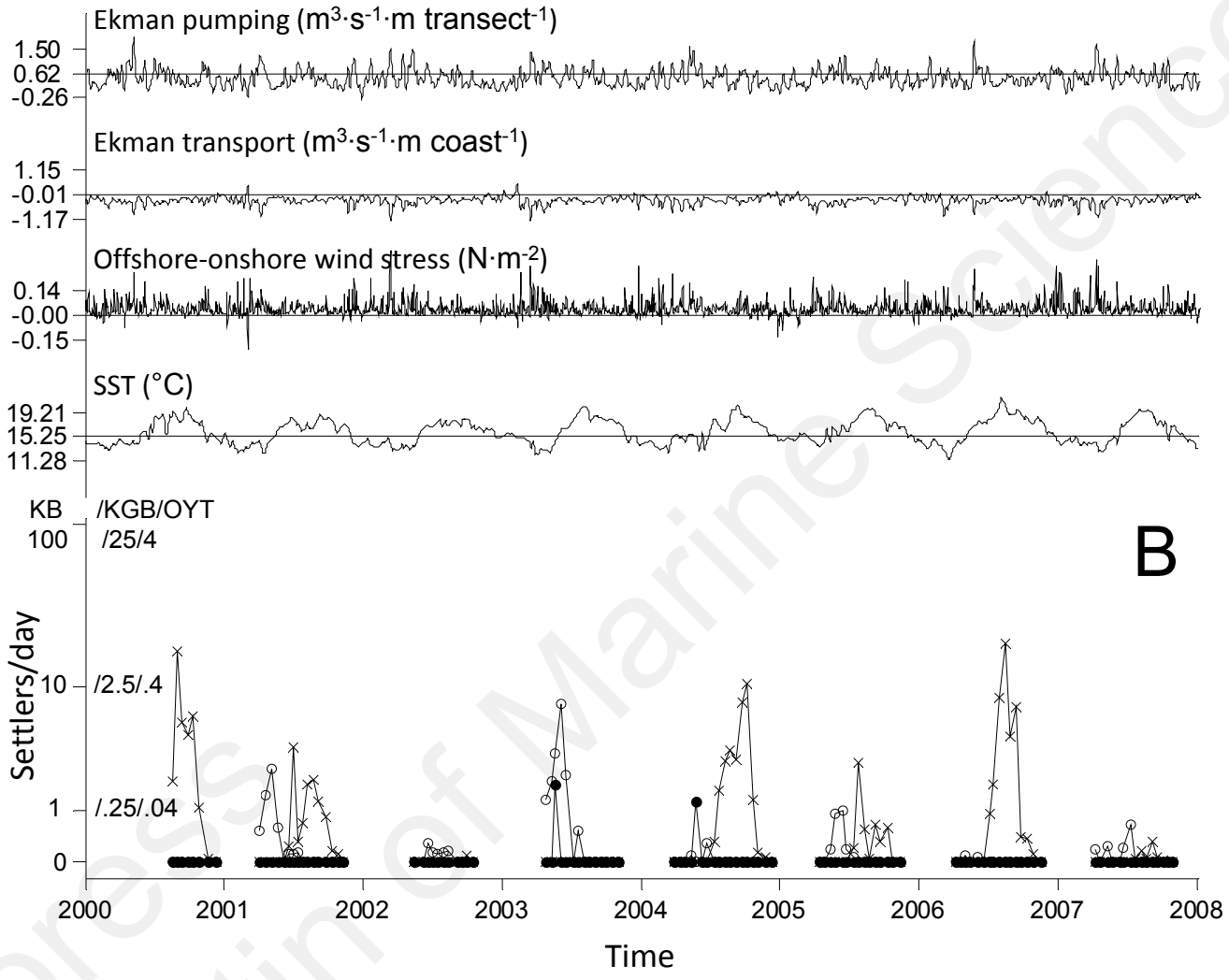

Figure S2. (B) Those for site 2.

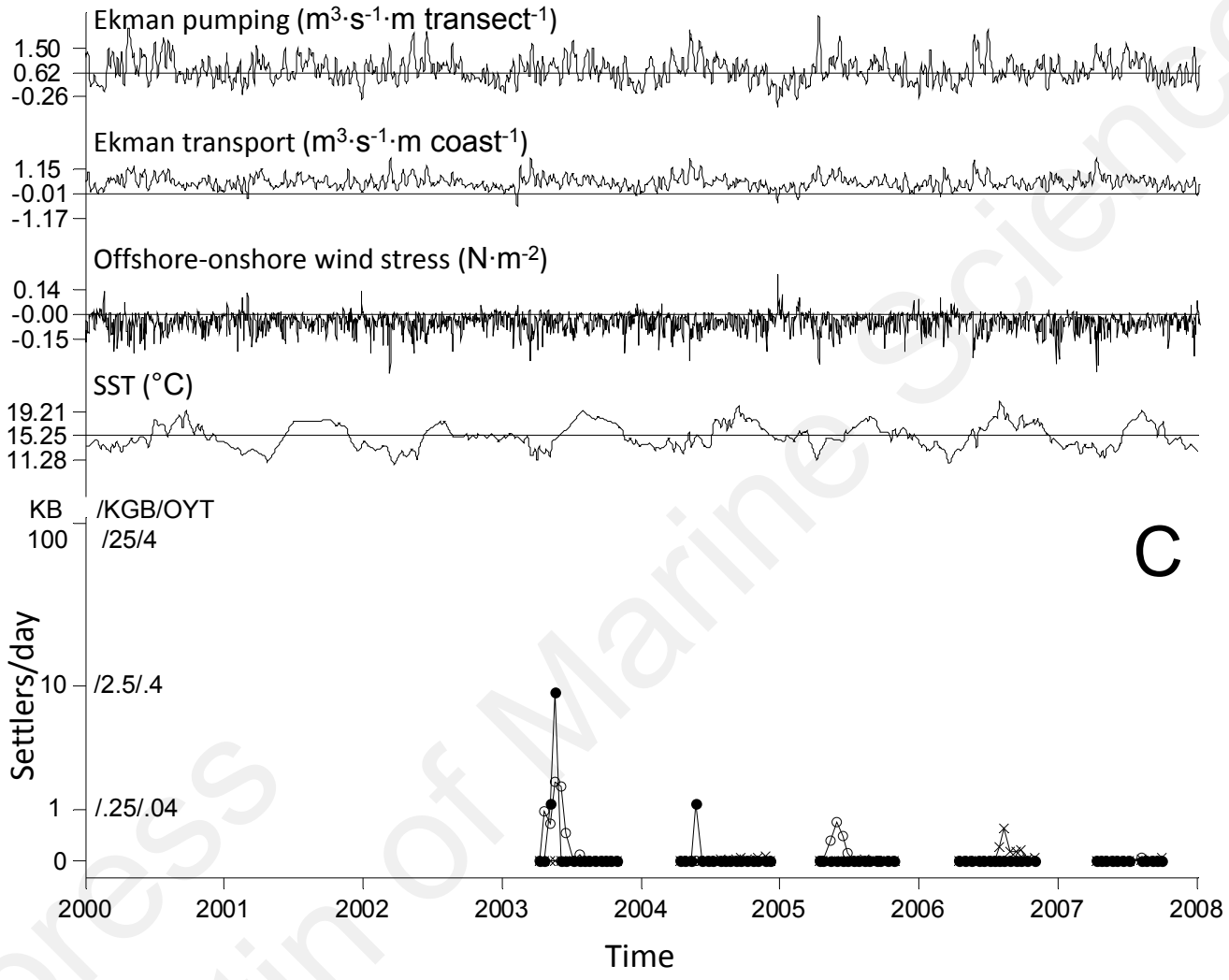

Figure S2. (C) Those for site 3.

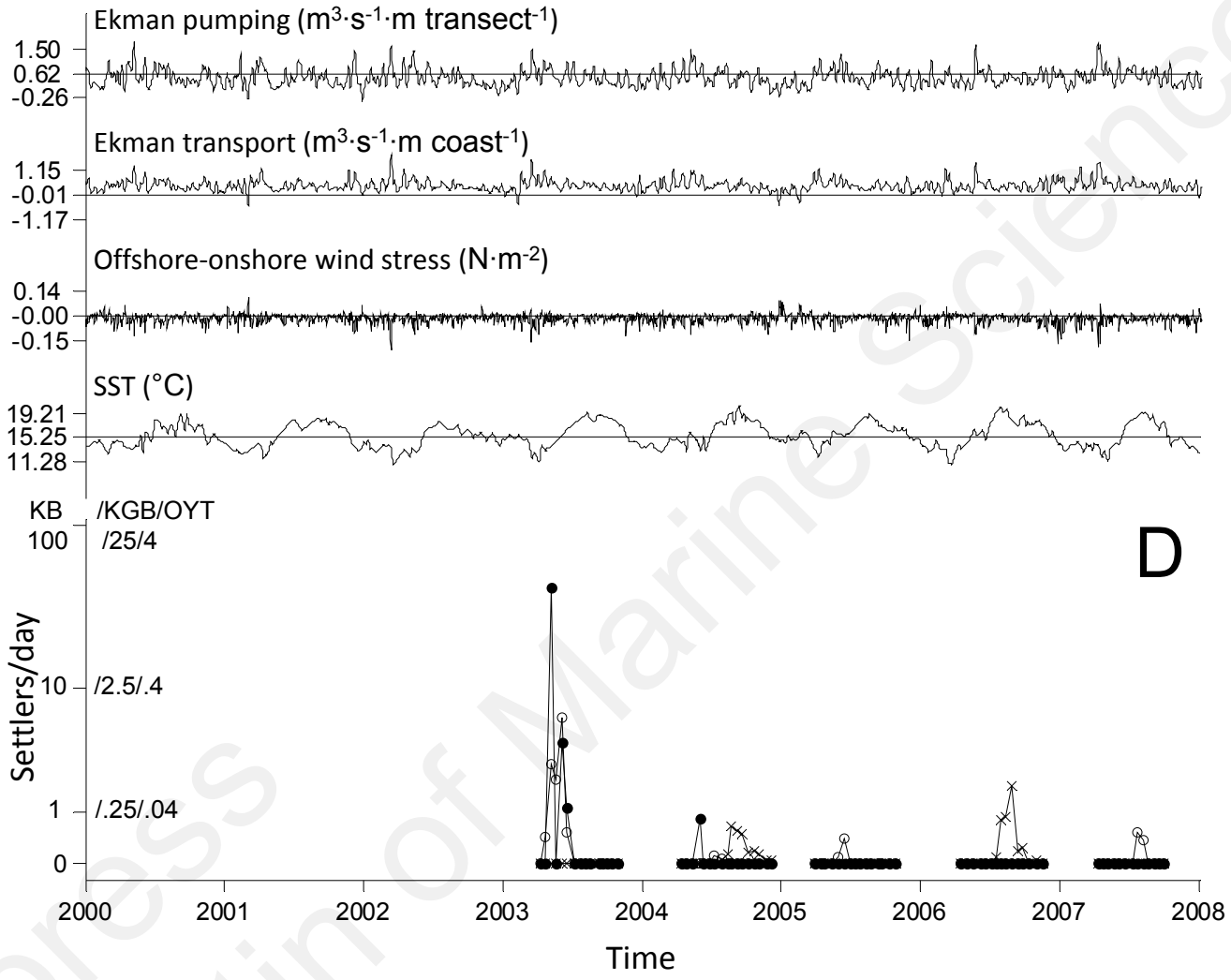

Figure S2. (D) Those for site 4.

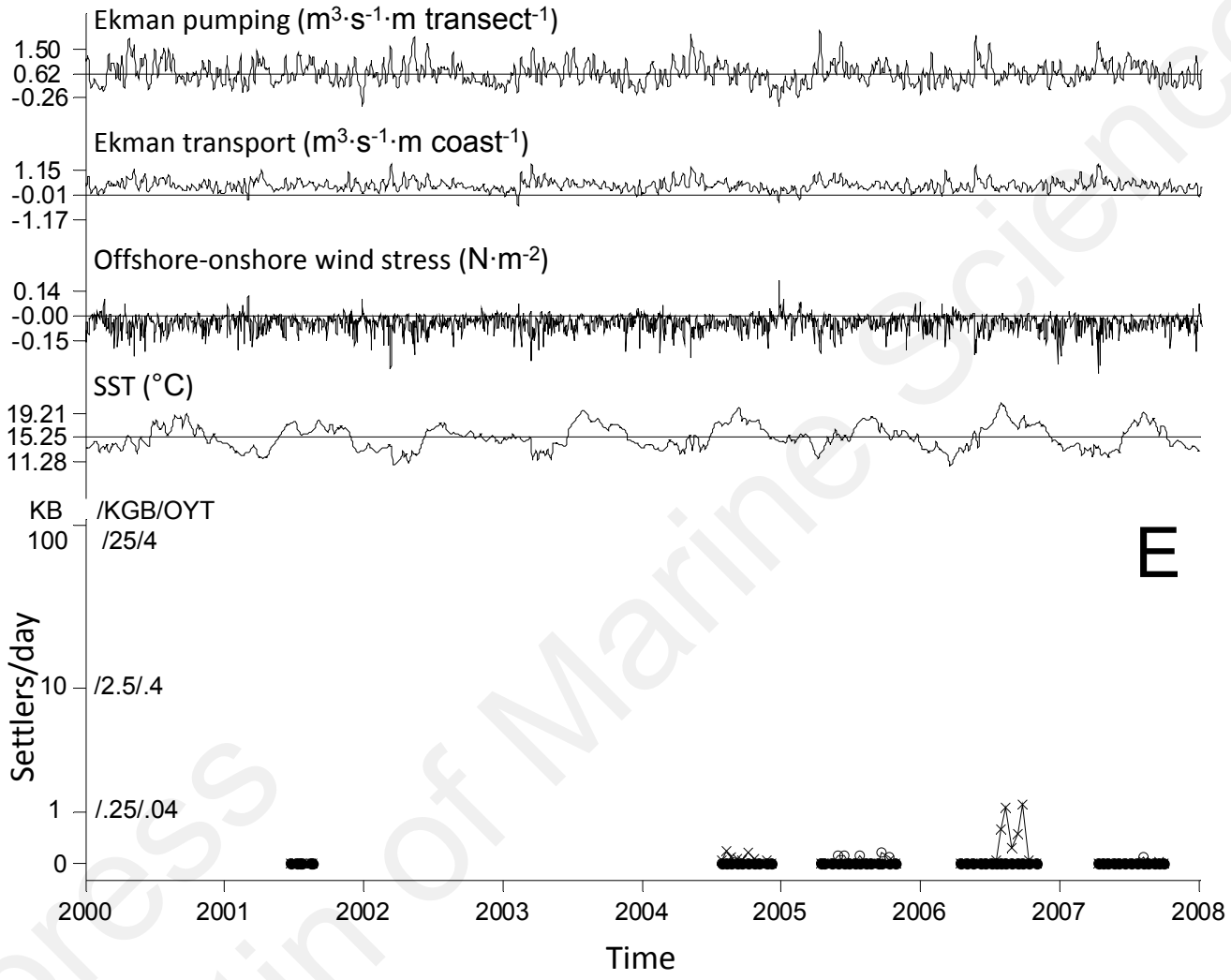

Figure S2. (E) Those for site 5.

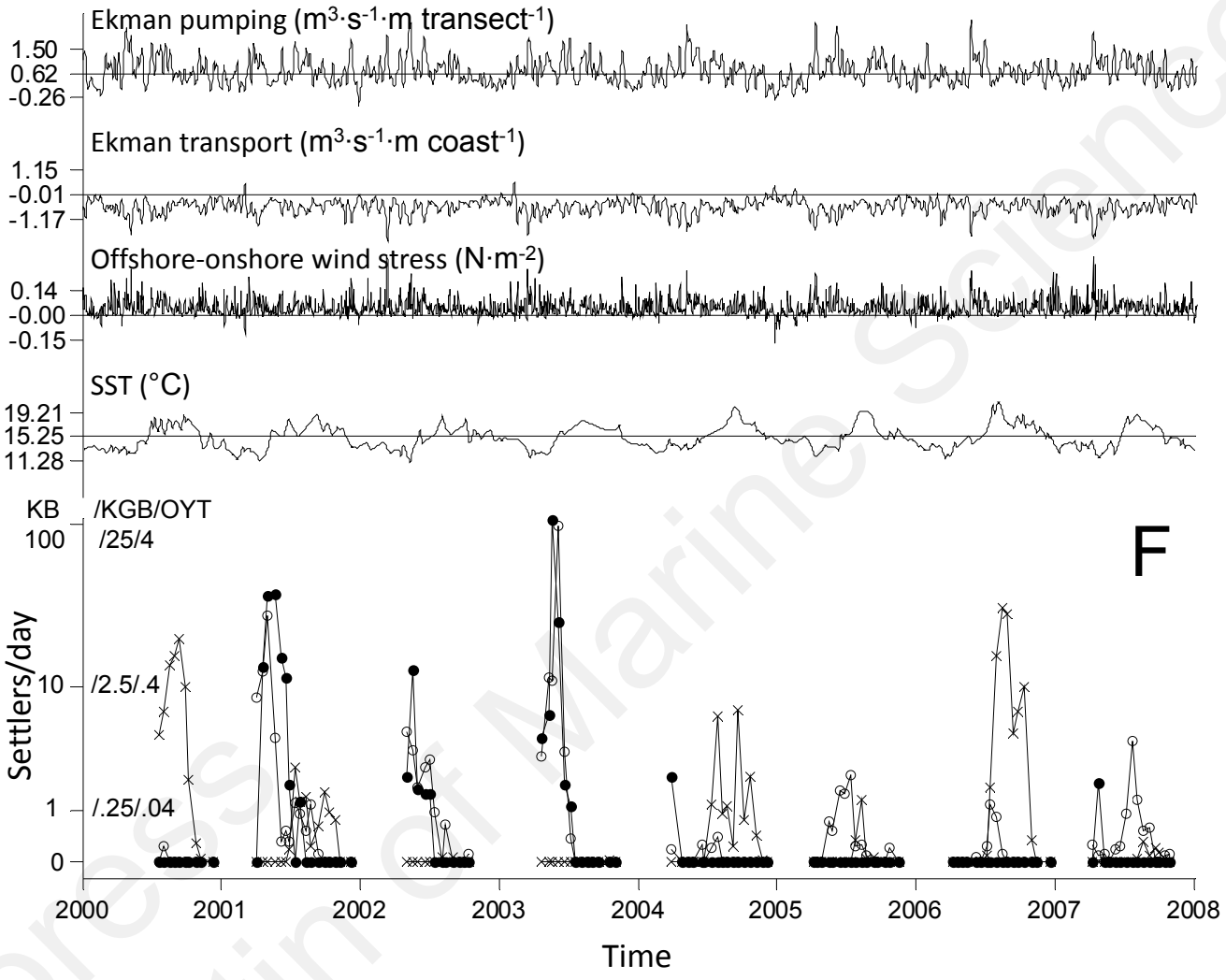

Figure S2. (F) Those for site 6.

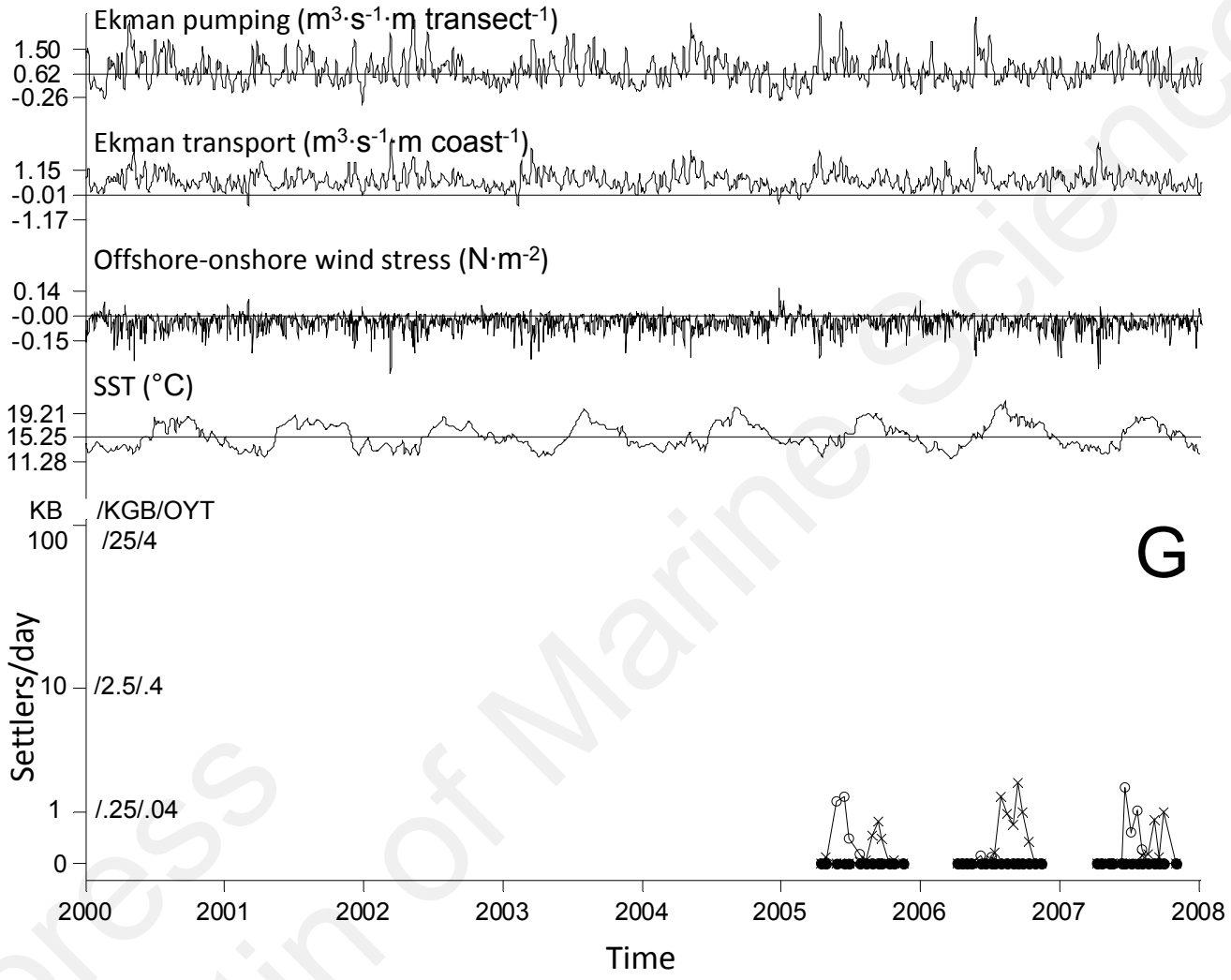

Figure S2. (G) Those for site 7.

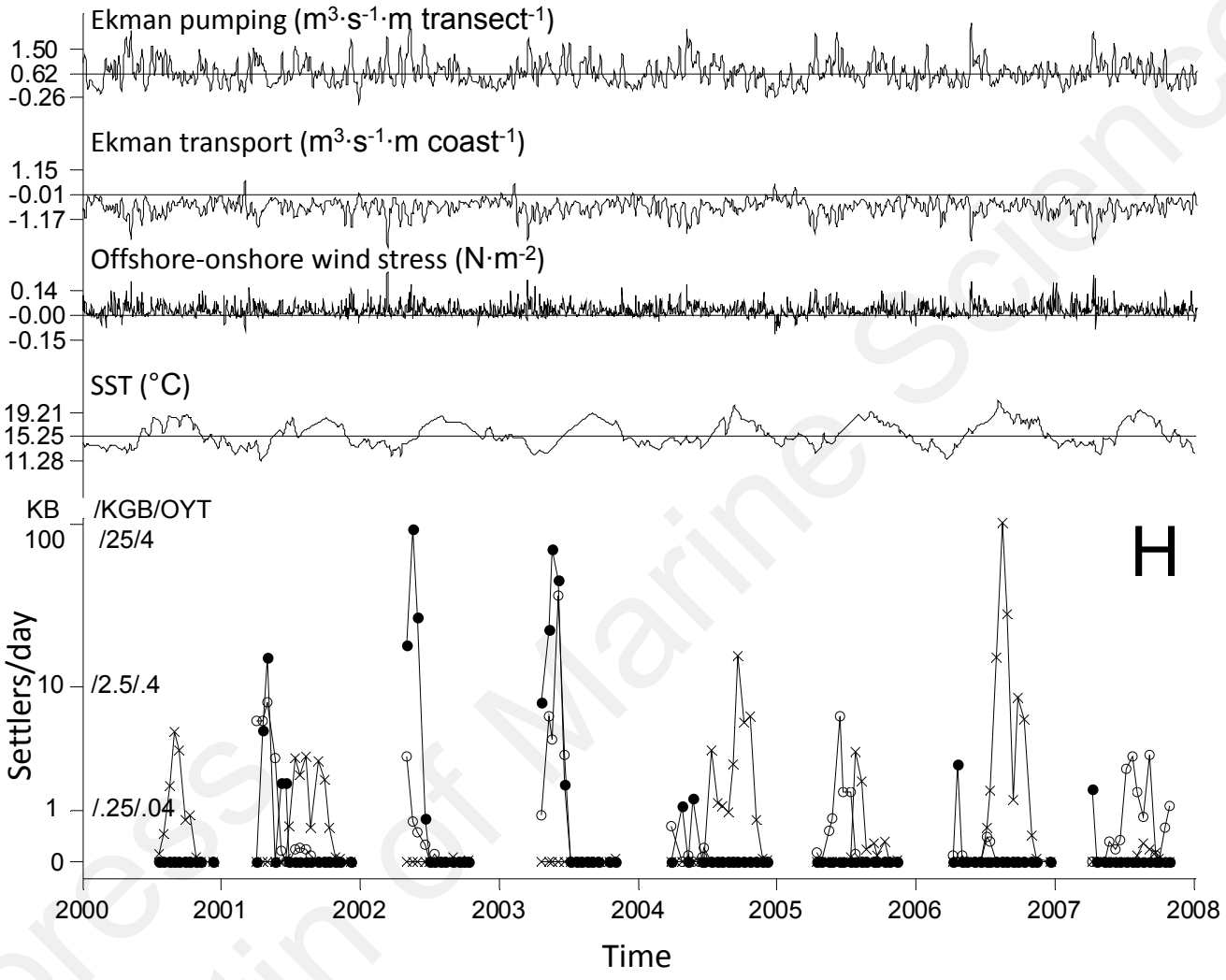

Figure S2. (H) Those for site 8.

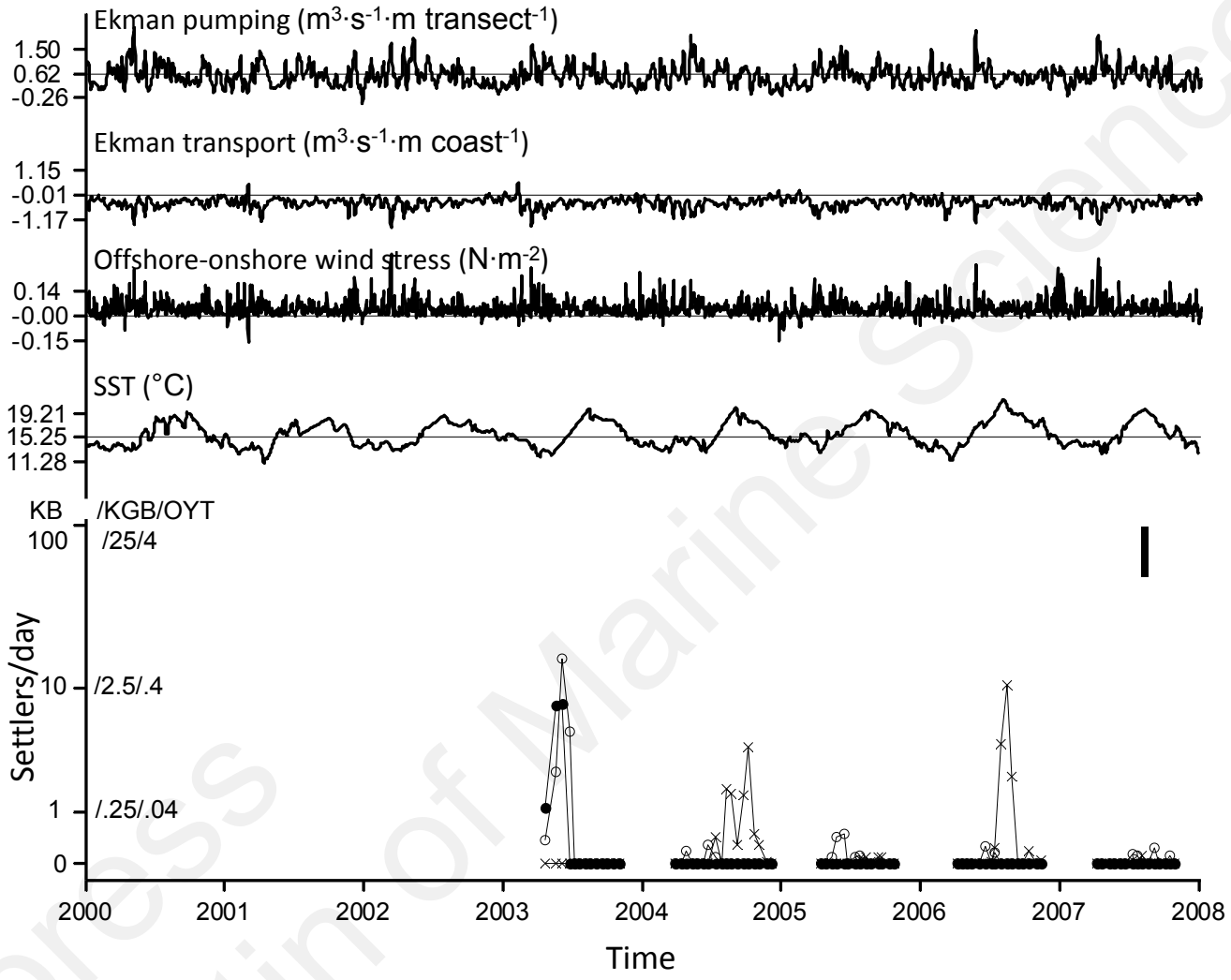

Figure S2. (I) Those for site 9.

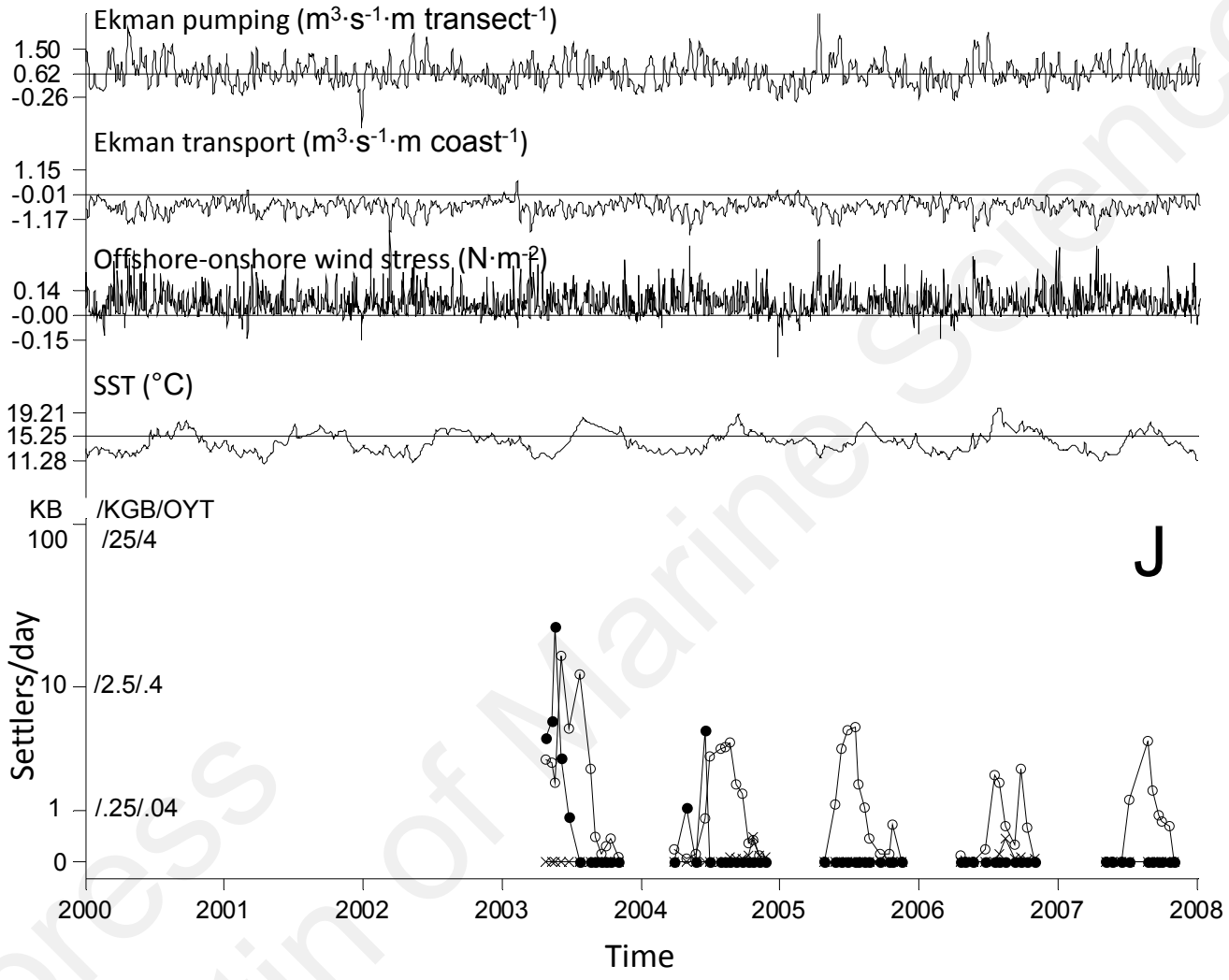

Figure S2. (J) Those for site 10.

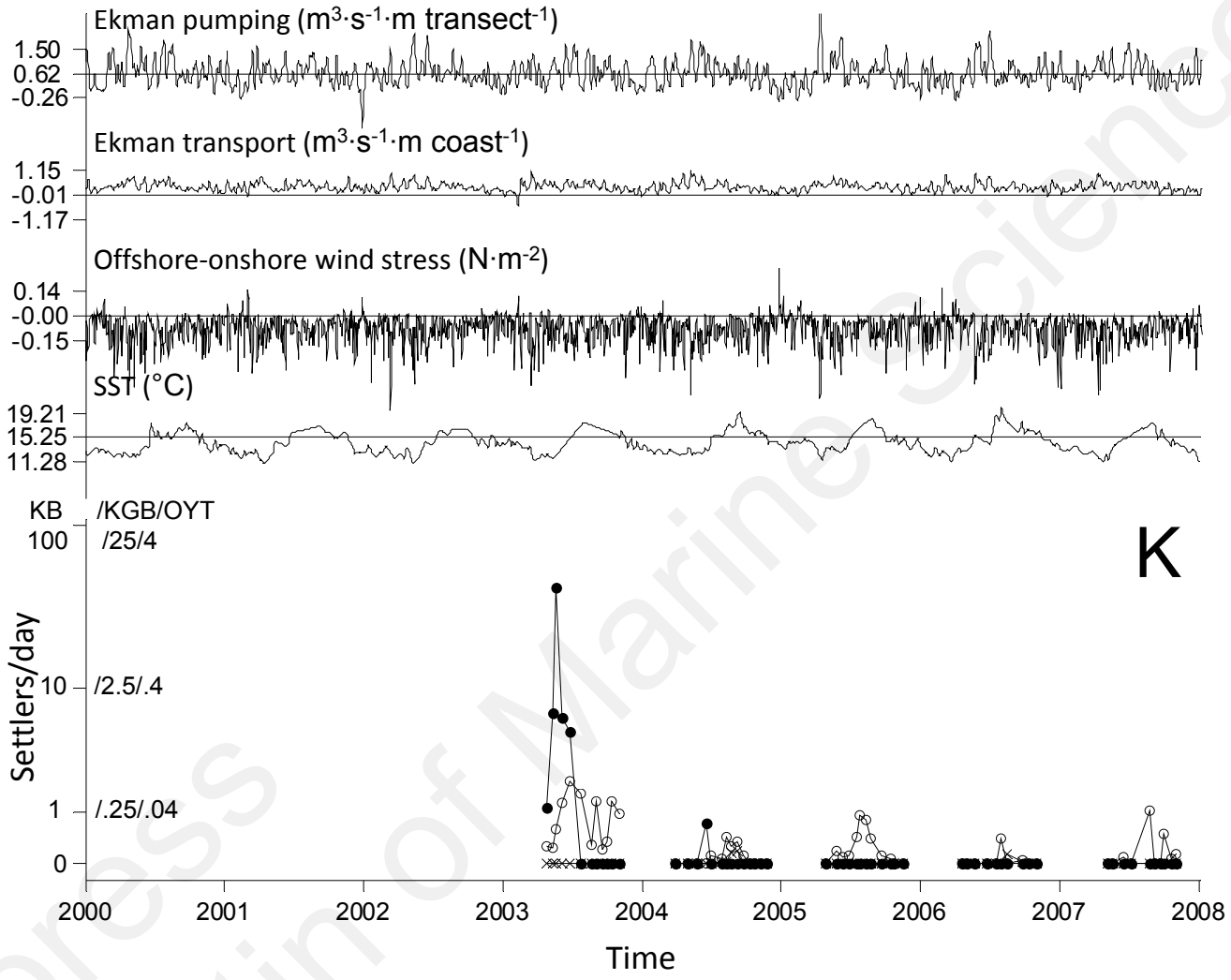

Figure S2. (K) Those for site 11.

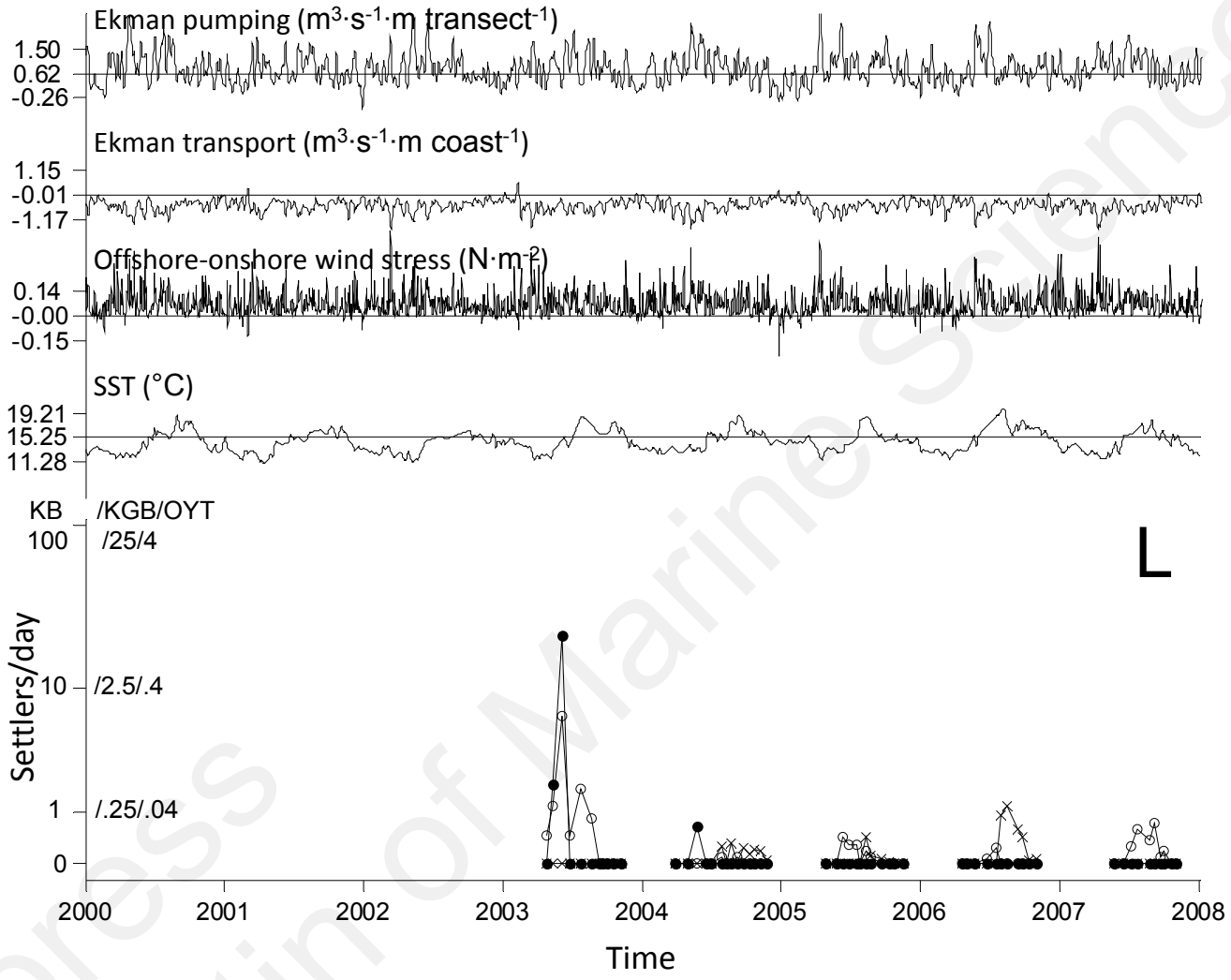

Figure S2. (L) Those for site 12.

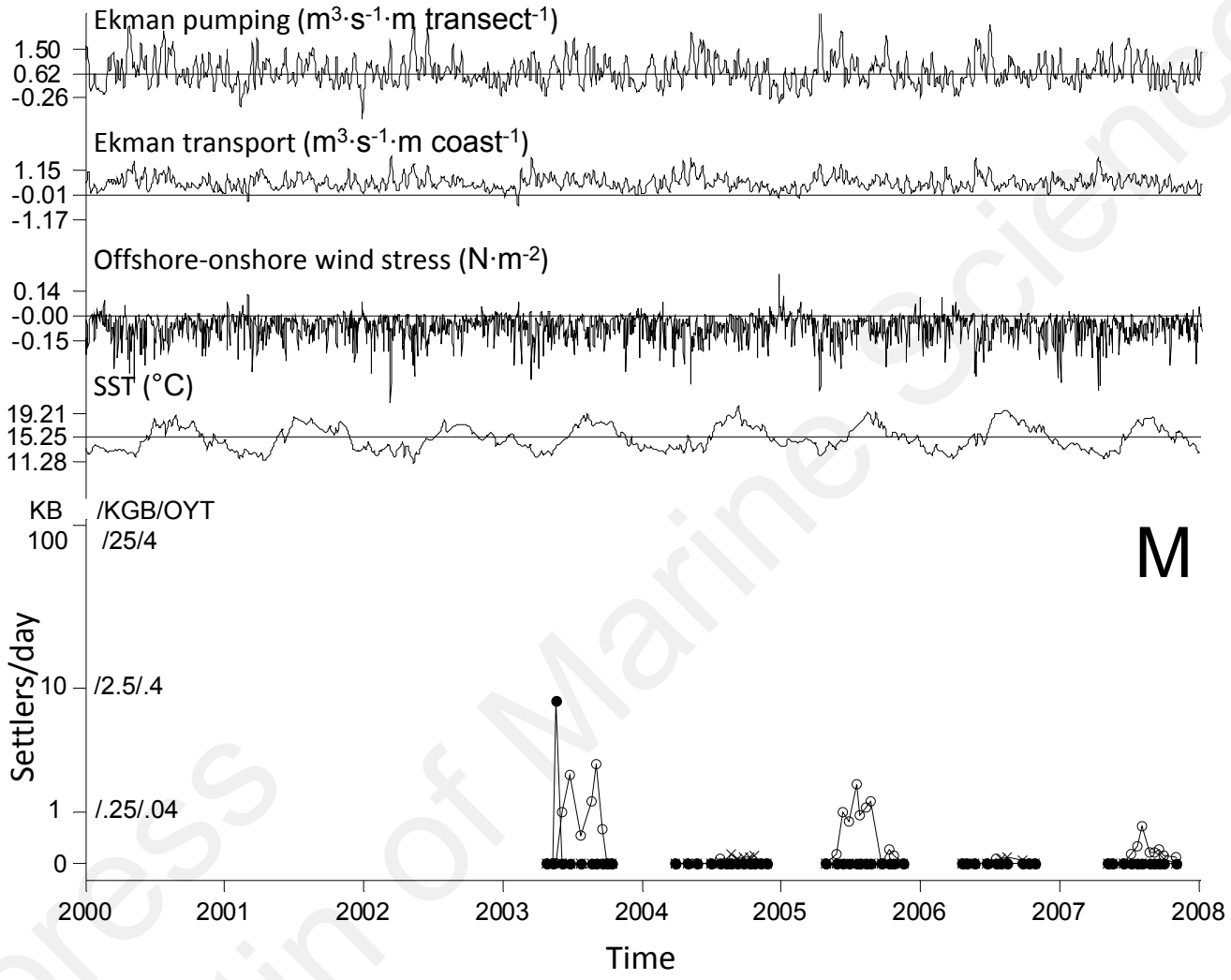

Figure S2. (M) Those for site 13.

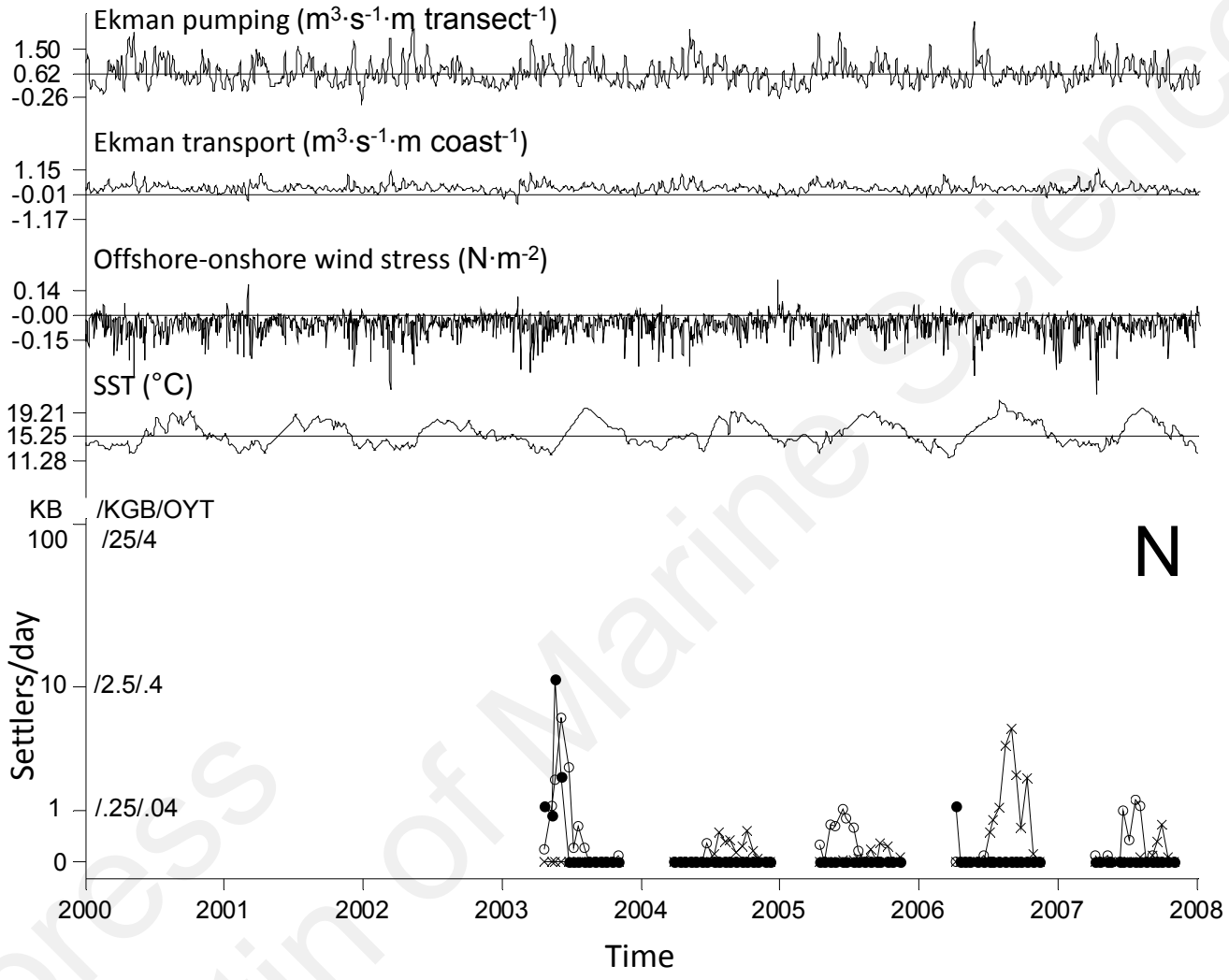

Figure S2. (N) Those for site 14.

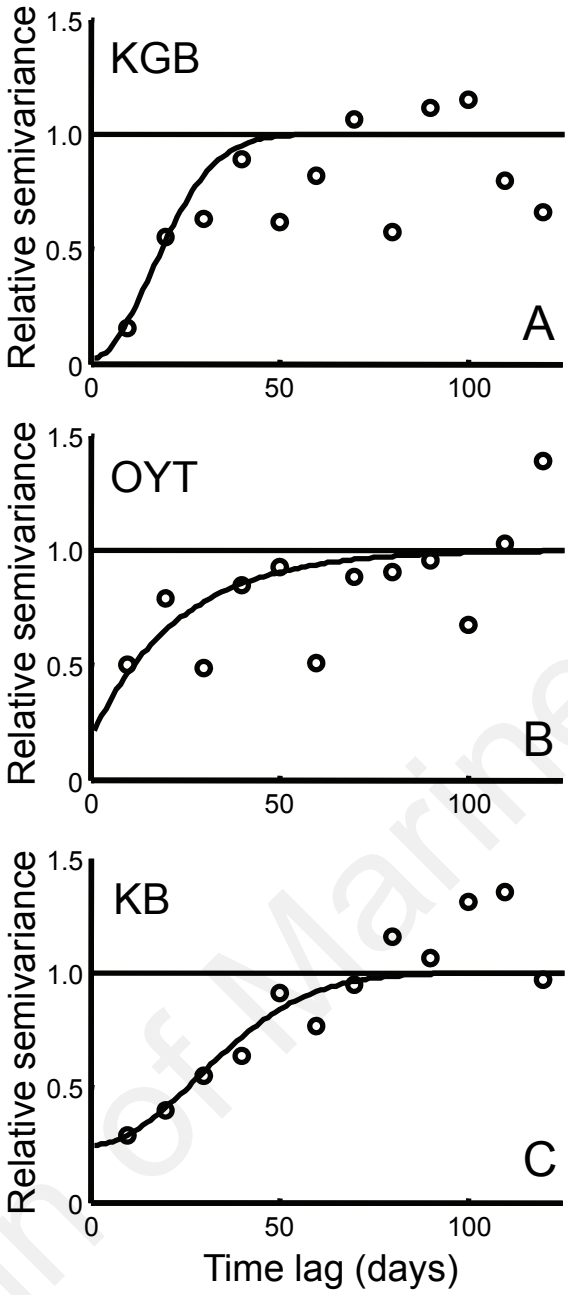

Figure S3. Semivariogram analysis of settlement time series. Sample (open circles) and model (solid lines) semivariograms on log10(x + 1)-transformed data for (A) KGB, (B) OYT, and (C) KB species groups. The model semivariograms, based on nonlinear weighted least-squares fits, were subsequently used in unconditional sequential Gaussian simulation to generate 1000 random autocorrelated null response data sets for Monte Carlo significance tests of regression models presented in the article. Models for each species, specified in terms of relative semivariance according to the conventions of Deutsch and Journel (1998): (A) Gaussian (range = 40 d, nugget = 0.02), (B) exponential (range = 70 d, nugget = 0.18), (C) Gaussian (range = 70 d, nugget = 0.25). Abbreviations as in Figure S2.